1990

Transition-Structure Recognition in Polyether-Catalyzed Ester Aminolysis Carried Out in Nonpolar Media.

John Charles Hogan
Louisiana State University and Agricultural & Mechanical College

Order Number 9123200

Transition-structure recognition in polyether-catalyzed ester aminolysis carried out in nonpolar media

Hogan, John Charles, Ph.D.

The Louisiana State University and Agricultural and Mechanical Col., 1990

U·M·I
300 N. Zeeb Rd.
Ann Arbor, MI 48106

TRANSITION-STRUCTURE RECOGNITION IN POLYETHER-CATALYZED ESTER AMINOLYSIS CARRIED OUT IN NONPOLAR MEDIA

A Dissertation

Submitted to the Graduate Faculty of the
Louisiana State University and
Agricultural and Mechanical College
in partial fulfillment of the
requirements for the degree of
Doctor of Philosophy

in

The Department of Chemistry

by
John C. Hogan
B.A., Rutgers University, 1976
December 1990

ACKNOWLEDGEMENTS

I wish to acknowledge the patient support of Dr. Richard David Gandour, in whose laboratories these studies were carried out. He had the wisdom required to stand aside and allow me the flexibility required to fully meet the objective I had set for myself. I also wish to acknowledge the electronic support of Mr. Les Edelin and Mr. Don Patterson, without whose skill and ingenuity this project would not have matured even to the point of allowing me to ask Nature the right questions, this being a fundamental prerequisite to producing relevant answers. I would like to thank Mark McLaughlin for a very thorough and painstaking proofreading job. Finally, I wish to acknowledge the support of Ms. Barbara Marquette, my word processor operator. The preparation of scientific manuscripts is a finicky endeavor, and Barbara is as good at it as anyone I've ever encountered.

To Rutgers University, which treated me like an intellectual water baby, and thus taught me to survive in a sink or swim world.

To Louisiana, a friend and kindred spirit, whose support in subtle ways helped me survive a considerable amount of pointless obstruction from an often rebellious but maturing and favorite adolescent offspring.

To Robert William Strozier, my first real mentor, a brilliant mind and a gentle being, who opened up a few profound scientific vistas for me, and enabled me to ground my chemical knowledge in a solid conceptual foundation.

To Isaac Newton, Ludwig Boltzmann, and Benoit Mandelbrot, whose mathematical work mapped out the space containing this conceptual foundation.

To Chester Morrison Dellinger, III, another mentor, who taught me the warrior's approach to challenge, and showed me the nature of the chameleon.

To Michael Allen Oliver, who taught me to solve a problem efficiently by first taking the shortest path to the heart of it and dotting the i's and crossing the t's later.

To Mary Jane Peters, my management mentor, a Cadillac doing a Volkswagen's job, who taught me that it is possible to solve problems quite effectively without understanding the issues involved, through the use of other people's expertise. Without her political and infrastructural support this work might never have been completed; and finally

To an unnamed friend, mentor, and benefactor, whose material, emotional, and moral support enabled me to climb a very rickety ladder to academic and personal accomplishment. Expediency demands that this benefactor remain unnamed.

TABLE OF CONTENTS

LIST OF TABLES

Page

LIST OF FIGURES

Page

LIST OF ILLUSTRATIONS

INSTRUMENTATION

60 MHz ^{1}H NMR spectra were recorded on a Varian A-60 spectrometer. 100 MHz ^{1}H FT-NMR spectra were recorded on an IBM NR/100 spectrometer. Gas-chromatographic analyses and purifications were performed on a GOW-MAC Model 350 Gas chromatograph equipped with a 5 ft x 0.25 in o.d., 15%, SE-30/Chromosorb P (60-80 mesh) semipreparative column. Melting points and micro-boiling points were determined with an Electrothermal capillary melting-point apparatus. Melting points and boiling points reported here are uncorrected. Kinetic runs were done with a Cary 118C UV/vis spectrophotometer equipped with a Varian Model 1829200 five-compartment sample changer. The spectrophotometer was interfaced to a Data General Nova 3 minicomputer via a Varian Model 310 data interface.

ABSTRACT

The mechanism of aminolysis of aryl acetates carried out in chlorobenzene involves rate-determining breakdown of the tetrahedral adduct formed by the nucleophilic attack of an amine on the carbonyl carbon of an aryl acetate ester. The breakdown of this tetrahedral adduct is assisted by the intervention of either a second amine moiety or a weakly basic catalyst moiety. The second amine or catalyst hydrogen bonds to an ammonium hydrogen of the zwitterionic tetrahedral adduct, which stabilizes this adduct by dispersing the positive charge on its cationic (ammonium) portion. Stabilization of the adduct occurs at the expense of a weaker 1,3-dipolar-stabilizing interaction that exists between the cationic ammonium region and the oxyanion region of this tetrahedral adduct. Breakup of this interaction by hydrogen-bonding bases destabilizes the oxyanion of the tetrahedral adduct, effectively raising the pK_a of the oxyanion. This facilitates expulsion of the aryloxide nucleofuge by the oxyanion in the rate-determining step. Aryloxide expulsion yields a hydrogen-bond-stabilized, N-protonated amide and aryloxide ion pair. An ammonium proton is subsequently shuttled from nitrogen to aryloxide in one or more fast steps to yield neutral products. A preassociation mechanism cannot be ruled out on the basis of available data. Preassociation involves attack by hydrogen-bonded amine dimer or amine-catalyst complex on ester to form the hydrogen-bond-stabilized tetrahedral adduct directly.

Glymes hydrogen bond their oxygens in pairs, in a bifurcated fashion, to each available ammonium hydrogen in the rate-determining transition structure for the reaction class. Glyme catalysis can be energetically dissected into bifurcation and bridging energies. Bifurcation is worth 1.2-1.4 kcal/mol and bridging between two ammonium hydrogens by catalyst is worth about 5 kcal/mol catalytically.

Triglyme binds all four of its oxygens in a bridged, doubly-bifurcated, hydrogen-bonding fashion, to the two available ammonium hydrogens of the rate-

determining transition structure in butylaminolysis, in either a "lock-and-key" or an "induced-fit" fashion. This work documents the first example of transition-structure recognition by glymes.

INTRODUCTION

1.1 Polyether Chemistry

Polyethers today come in a bewildering variety of flavors. Some of the names of general classes of polyethers bandied about in the recent literature include coronands, podands, spherands, hemispherands, cavitands,[1] open chain cryptands, podocoronands, and octopus molecules.[2] This dissertation will restrict itself to discussions involving crown ethers, CRN(n) (a subset of coronands), glymes, GLM(n) (a subset of podands), and α,ω-dimethoxyalkanes, DME(n) (a subset of podands).

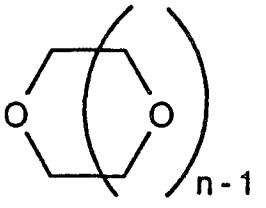

CRN (n)

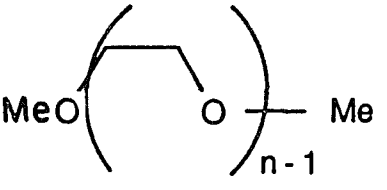

GLM (n)

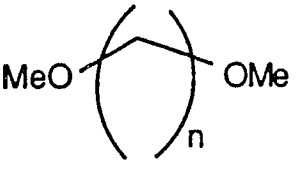

DME (n)

Although the ability of glymes to dissolve metal salts was recognized by Wilkinson in 1959, interest in polyethers as ionophores did not really begin to demand intense fascination from the chemical community until 1967, when Charles Pedersen discovered the ability of crown ethers as additives to dissolve ionic salts in nonpolar solvents,[3] with the concomitant production of extremely reactive anionic species.[4] This discovery, which earned Pedersen the 1988 Nobel Prize in chemistry, has been called "the shot heard 'round (sic) the [chemical] world".[1]

Until about 1980 the major thrust of polyether research seems to have been an attempt to develop as many different flavors of cyclic and polycyclic polyethers and polyether analogs as possible, with a view toward optimizing the formation and utility of the reactive anionic species produced by the reaction of polyethers with alkali metal

salts.[1,5,6] Liotta and Harris have coined the term "naked anions"[7] to describe the reactive anionic species produced in this manner. Crown ethers and more complicated polyethers form naked anions by encapsulating cations of alkali metal salts into their interiors as shown in Figure 1.[4] Electron density from crown ether oxygen lone pairs solvates an encapsulated cation, weakening its bonding to the anionic counterion of a dissolved alkali metal salt molecule. The exterior surface of the crown-cation complex is hydrophobic, making the complex soluble in nonpolar media. The associated anion is dragged into solution along with the crown-cation complex, and is only weakly solvated by this complex. The poor solvation experienced by anions in this predicament makes these anions highly reactive toward Lewis-acidic sites of substrate molecules, especially in nonpolar media.[4] Naked anions have proven their utility in a wide variety of reactions and applications, including nucleophilic aliphatic and aromatic substitutions, eliminations, decarboxylations, Michael additions, base-catalyzed ester hydrolyses, sigmatropic rearrangements, dichlorocarbene generation, oxidations, reductions,[5] and phase-transfer catalyzed reactions.[8]

Crown ethers are generally considered to be much better ionophores than glymes.[1] This is thought to be due to a structural attribute known as preorganization.[6] The extent to which the conformation of an uncomplexed ligand resembles the conformation of the same ligand fragment after it has formed a complex with a cation is the extent to which the ligand is said to be preorganized. Glyme complexes of metal ions have been shown by x-ray crystallography[9] to resemble crown ether complexes of metal ions. Metal ions wrap glymes around themselves during binding, forcing these ligands to adopt conformations similar to conformations already built in to crown ethers by virtue of their macrocyclic natures. There is some non-crystallographic evidence that the same phenomenon occurs in glyme complexation of diazonium ions.[10] The foregoing demonstrates that crown ethers are more preorganized than glymes toward

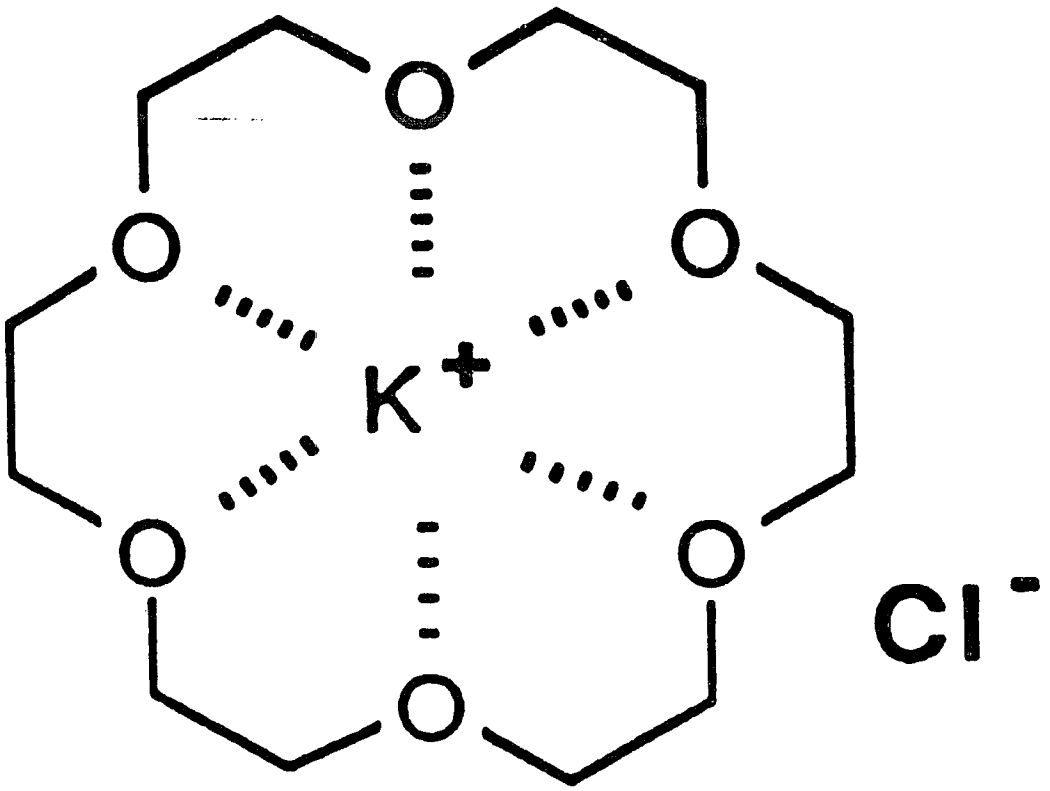

Figure 1. 18-Crown-6 potassium chloride complex.

metal and diazonium ion binding. Crown ethers are generally believed to be more preorganized than glymes toward binding to most cations.[1]

In "host" (ligand)-"guest" (cation or other species bound to a multidentate ligand) chemistry,[11] macrocyclic hosts (like crown ethers) tend to form stronger complexes with most guests than do analogous open-chain hosts (like glymes).[1] This effect is called the macrocyclic effect.[12] With respect to crown ether vs. glyme binding, the macrocyclic effect has been shown to apply to metal ion,[13] primary ammonium ion,[14] and diazonium ion[10] guests. The macrocyclic effect may not apply to secondary ammonium ion guests.[14] In fact, secondary ammonium ion guests may show an inverse macrocyclic effect[15] in nonpolar media. As implied in the previous paragraph, the macrocyclic effect, where operative, is generally believed to be caused by macrocyclic preorganization.[1]

Since about 1980 polyether research has taken off in many different directions. Some of the topics currently under investigation include anion-complexing hosts (anion cryptates),[9] uncharged guest molecules,[16] chromogenic indicators for metal ions,[17] photocontrolled ion extractions,[18] polymer-bound polyethers,[19] chiral recognition,[14] enzyme modeling,[20] and a renewed interest in glymelike species as inexpensive phase-transfer catalysts,[8] selective ion-binding agents,[2,21] PCB and dioxin detoxifiers,[22] and homogeneous reaction catalysts for reactions involving ionic intermediates and transition structures.[10,14,15] Curiously, the current interest in glymes arose out of the excitement generated by crown ether chemistry, even though glymes are generally considered to be poorer ionophores than crown ethers.[8] Apparently the original impetus for this came from the recognition that even though crown ethers are more powerful phase-transfer catalysts than glymes on a molar basis, glymes are far more effective on a cost basis.[8]

Of all of the current areas of activity in polyether chemistry the use of polyethers as homogeneous reaction catalysts is of most relevance to the remainder of the work

discussed here. While transition-structure recognition by crown ethers in homogeneous transacylations of amino ester salts has been demonstrated by Chao and Cram,[14] and also by Saski and Koga,[20] the experimental results detailed in this dissertation provide the first example of transition-structure recognition by glymes. This glyme work also provides the first clear example of transition-structure recognition by polyethers in which the polyether catalysts accelerate reactions by direct manipulation of reaction electronics and electrostatics rather than by manipulating molecular proximity. This point will be discussed in more detail later in this work.

1.2 Aminolysis of Aryl Acetates in Chlorobenzene: The Benchmark Reaction

The experimental work in this dissertation involves measurement of the catalytic activities of polyethers. The polyether catalysts under study accelerate the rates of reactions in aryl acetate aminolysis carried out in chlorobenzene. The methodology used to study catalysis of this benchmark reaction class has been worked out by Su and Watson,[23] who discovered that the catalytic activities of a variety of oxygen and nitrogen bases parallel their hydrogen-bonding abilities and not their basicities in catalysis of the butylaminolysis of 4-nitrophenyl acetate.

Nagy and coworkers[24] have generalized the demonstration of the hydrogen-bonding nature of catalysis of ester aminolysis in aprotic media to include a variety of aprotic solvents, benzoate and cinnamate ester substrates, and a variety of amine catalysts and nucleophiles. A diversity of experimental evidence has demonstrated conclusively[23-26] that ester aminolysis occurs via a zwitterionic tetrahedral intermediate like $T^{\pm}$ (for primary amines reacting with aryl acetates), which is formed by attack of an amine nucleophile on the carbonyl carbon of an ester. Formation of $T^{\pm}$ is rate-limiting in protic solvents. Breakdown of this intermediate is rate-limiting in aprotic solvents.

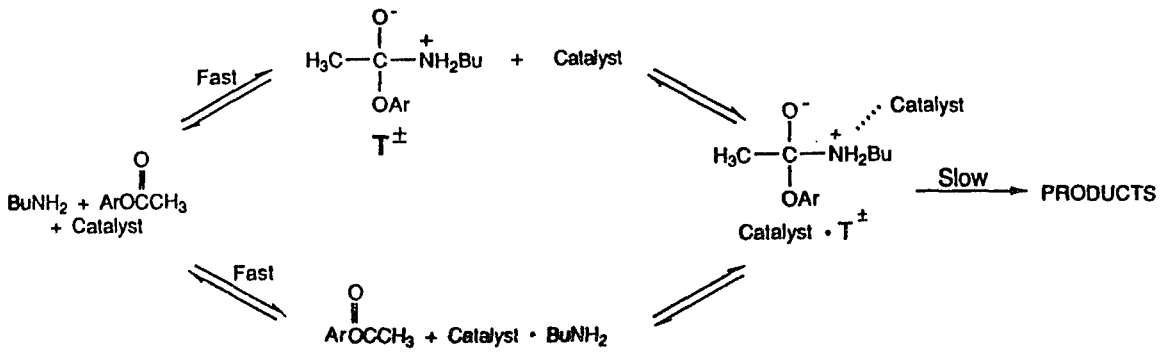

The observed rate law for ester aminolysis in aprotic solvents at 25° is:[23,24] rate = k_{obs} [ester], where $k_{obs} = k_0$ [amine]$^2 + k_{cat}$ [amine] [catalyst], such that k_{obs} is a pseudo-first-order observed rate constant (excess amine), and k_{cat} is the catalytic rate constant (or activity) of any nitrogen or oxygen containing weak base capable of hydrogen bonding to a hydrogen-bond donor. The fact that amines all show the same catalytic activity vs. hydrogen bonding ability behavior as other bases used to catalyze this reaction class[24] suggests that the first term in the rate law is second order in amine because a second molecule of amine performs the hydrogen-bonding function of a catalyst in the "uncatalyzed" mechanism. Thus the rate law shows that the rate-determining transition structure for ester aminolysis in aprotic media is composed of a $T^{\pm}$-like component (made from one amine nucleophile piece and one ester piece) and a hydrogen-bonding "catalytic" component (which is either a second amine molecule or some other base in the system).

Given the structure of $T^{\pm}$ it seems likely that the region a hydrogen-bonding base catalyst interacts with is the ammonium ion piece of this zwitterion. Menger and Vitale showed[26] that tetrahexylammonium benzoate catalyzing aryl ester aminolysis in toluene is capable of causing the rate-determining step of the reaction to change from breakdown of tetrahedral intermediate (aprotic media chemistry) to formation of tetrahedral intermediate (protic media chemistry). These workers concluded that benzoate abstracts an ammonium proton from the tetrahedral intermediate in the reaction path enabling the oxyanion of this zwitterion to expel nucleofuge without yielding a high energy N-

protonated amide. This suggests that protic solvents may be capable of deprotonating the ammonium ion of $T^{\pm}$ (or allowing amine or base catalyst to do so), whereas in aprotic media the ammonium ion of $T^{\pm}$ may remain ionized, forcing catalysts to stabilize this ion to the extent they can, by hydrogen bonding to it, until the oxyanion of $T^{\pm}$ expels nucleofuge. Aryloxide expulsion would thus yield catalyst-stabilized N-protonated amide in aprotic media and neutral amide in protic media. In aprotic media catalyst-stabilized N-protonated amide would then shuttle an ammonium proton to nucleofuge to yield neutral reaction products in one or more subsequent fast steps. Because rate-determining breakdown of $T^{\pm}$ in aprotic media is catalyzed by hydrogen-bonding bases it seems reasonable to suppose that catalysts function by hydrogen bonding to one or more ammonium hydrogens in $T^{\pm}$, as well as in the rate-determining transition structure immediately following $T^{\pm}$ on the reaction path, and also in PA^{+} (the N-pronated amide following nucleofuge expulsion). Catalytic hydrogen bonding should stabilize all three of these species; reaction rate enhancements are due to stabilization of the (rate-determining) transition structure lying between $T^{\pm}$ and PA^{+} on the reaction path in this scenario.

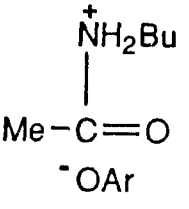

PA^{+}

The experimental results outlined in this dissertation show that base catalysts do indeed hydrogen bond to one or more ammonium protons in $T^{\pm}$, PA^{+} and the intervening transition structure. Furthermore, the nature and qualitative geometry of

hydrogen bonding by polyether catalysts to these three species is demonstrated in this work.

EXPERIMENTAL PROCEDURES

2.1 Synthetic Materials

2.1.1 Pentaglyme

To 2.00 g (7.93 mmol) of pentaethylene glycol monomethyl ether (Parish Chemical Co.) was added 4 g of sodium hydroxide (Holcross Chemical technical grade) and 20 mL of dry dioxane (freshly distilled from molten metallic sodium). This mixture was stirred at reflux for 1 h, after which 2.00 g (15.9 mmol) of dimethyl sulfate (Aldrich Chemical Co.) was added dropwise, producing a vigorous reaction. The reaction mixture was refluxed for 1 h, cooled to room temperature, and partitioned between 50 mL of dichloromethane and 30 mL of water. The resulting organic layer was washed twice with 50 mL each time of distilled water, dried (magnesium sulfate), concentrated at reduced pressure (rotary evaporation using water aspirator), and stirred over molten sodium metal for 1 h. The excess sodium was then removed from the resulting brown gelatinous suspension, and the suspension was bulb-to-bulb (Kugelrohr) distilled under 1.0 Torr pressure in a 150° oven (lit.[27] bp 153-155° (3 Torr)), yielding approximately 0.5 g of a dark brown solid and 1.44 g (68.2%) of a water-white oil whose ^{1}H NMR and TLC were consistent with pure pentaglyme (R_f 0.37, 1:9 2-propanol/hexanes); ^{1}H NMR (CCl_4, 60 MHz) δ 3.29 (s, 6 H), 3.32-3.67 (m, 20 H).

2.1.2 Octaglyme

A sample of 18.0 g (92.7 mmol) of tetraethylene glycol (Aldrich Chemical Co.) was mixed with 100 mL of pyridine (Reilly Chemical) in an ice bath. 30.0 mL (44.4 g, 388 mmol) of methanesulfonyl chloride (Aldrich Chemical Co.) was slowly added to this mixture with swirling. The resulting reaction was quite exothermic; the reaction temperature was kept below 25°. The reaction mixture was stored at -20° overnight,

after which it was poured onto 100 g of cracked ice, and extracted with 200 mL of dichloromethane. The resulting organic layer was washed with 200 mL of cold 6 *N* HCl, followed by 200 mL of saturated sodium bicarbonate. The organic layer was then dried (magnesium sulfate), filtered, concentrated, and allowed to lose residual solvents under reduced pressure (1.0 Torr) overnight, yielding 32.5 g (92.8 mmol, 100%) of a bright orange oil whose ^{1}H NMR was consistent with pure tetraethylene glycol dimesylate. 20 g of metallic sodium ribbon (Aldrich Chemical Co.) was pressed into a reaction vessel containing 100 mL of tetrahydrofuran (QO Chemical Co.) which was freshly distilled from sodium ribbon. To this mixture was added a solution composed of 25.0 g of diethylene glycol monomethyl ether (Aldrich Chemical Co.) and 75 mL of tetrahydrofuran. The addition was done over a period of 30 min, with stirring. The resulting reaction mixture was refluxed for 2 h, after which it was cooled in an ice bath, and a solution of tetraethylene glycol dimesylate (prepared as described above) dissolved in 75 mL of tetrahydrofuran was added over a period of 30 min. The resulting reaction mixture was warmed to room temperature and then refluxed for 2 h. The liquid portion was then decanted away from the remaining sodium ribbon, and added, with swirling, to 20 mL of water, yielding a light yellow liquid above a white precipitate. The liquid layer was filtered, dried ($MgSO_4$), filtered again, and concentrated (rotary evaporation using water aspirator), yielding ≈ 40 g of a dark yellow oil. A colorless material (8 mL) was distilled away from the oil at reduced pressure (0.07 Torr), bp 32-120°. The remaining oil was distilled at reduced pressure three times after stirring over molten sodium for 2 h each time. The final distillation yielded 10.8 g (28.7%) of a colorless oil, bp 190° (0.1 Torr). A 1.00 g portion of this material was chromatographed on a 20 x 20 cm glass-backed 60 Å silica gel TLC plate (1 mm layer thickness, E-M Science) with 10% 2-propanol/hexanes yielding two fractions: R_f 0.26, ≈ 85% (visual density); R_f 0.39, ≈ 15% (visual density). The lower fraction (R_f 0.26) was scraped away from

the plate and extracted three times with acetone (20 mL each time). The combined extracts were filtered, concentrated, and distilled from molten sodium yielding 0.432 g of clear oil, bp 190° (0.1 Torr), lit.[28] bp 215-218° (0.45 Torr), whose ^{1}H NMR and TLC were consistent with pure octaglyme (R_f 0.25, 1:9 (v/v) 2-propanol/hexanes): ^{1}H NMR (CCl_4, 60 MHz) δ 3.28 (s, 6 H), 3.35-3.64 (m, 32 H).

2.1.3 Lower-series Diethers

The α,ω-dimethoxyalkane series DME(3) through DME(5), members of which are generically referred to hereinafter as lower-series diethers, was obtained by treating the corresponding α,ω-diols with excess sodium hydride and iodomethane. (See Table I for quantities of materials used and isolated.) Three samples of excess sodium hydride-oil dispersion were weighed out in three-necked reaction flasks, and each sample was washed, with stirring, five times, with 25 mL each time of pentane. Pentane washes were decanted and discarded after stirring was discontinued and solid material given time to settle. The reaction flasks were then charged with 75 mL each of dry ether followed by 5.00 g of the α,ω-diol corresponding to the target diether. The resulting three-phase (one solid and two liquid phases) mixtures were stirred at reflux overnight, during which time they became two-phase (one solid and one liquid phase) mixtures. To each of the resulting reaction mixtures was added a solution of excess iodomethane (MeI) dissolved in 25 mL of dry ether. These mixtures were then stirred at reflux for 8 h, after which they were cooled to room temperature without stirring, yielding a series of three two-phase (one clear liquid and one white solid phase) mixtures. Each of the resulting liquid organic phases was decanted away from remaining solid material. The remaining solids were then washed twice with 50 mL each time of dry ether, and washes were combined with the liquids which had previously been decanted away from the reaction solids in the corresponding reaction

vessels. The resulting liquids were filtered separately through glass frits and fractionally distilled, yielding the target α,ω-dimethoxyalkanes (lower-series diethers). These diethers were further purified by preparative gas chromatography on a 5-ft, 15%, SE-30/Chromosorb P (60-80 mesh) column using a GOW-MAC Model 350 gas chromatograph. All of the resulting purified lower-series diethers were at least 97% pure by GC analysis, and ^{1}H FT-NMR spectra (100 MHz, $CDCl_3$) were consistent with the pure target compounds. Boiling points were in good agreement with literature values. The final isolated yields and observed boiling points of these lower-series diethers are given in Table I.

Table I. Synthetic parameters for lower-series diether preparations.

	DME(3)	DME(4)	DME(5)
wt, g (meq) diol used	5.00(156)	5.00(111)	5.00(96.0)
wt, g (meq) NaH/oil used	15.0(313)	11.0(229)	11.0(229)
wt, g (meq) MeI used	45.0(317)	35.0(247)	35.0(247)
wt, g (meq) diether	1.99(43.2)	2.39(40.1)	3.66(55.4)
isolated yield	27.7%	36.2%	58.0%
bp, °C	105.3	131.5	159.2
lit. bp, °C	105.5[a]	132[b]	157-157.5[c]

[a] Reference 29. [b] Reference 30. [c] Reference 31.

2.1.4 Higher-series Diethers

The α,ω-dimethoxyalkanes DME(6) through DME(12) except DME(11), members of which are generically referred to hereinafter as higher-series diethers, were synthesized via intermediate α,ω-ditosylates derived from the corresponding α,ω-diols. α,ω-Ditosylates treated with sodium methoxide in methanol yielded the corresponding α,ω-dimethoxyalkanes. (See Table II for quantities of materials used and isolated.) Six Erlenmeyer flasks were charged with 50.0 mL (618 meq) each of pyridine (excess) and 5.00 g each of the α,ω-diol corresponding to a given target diether and cooled to 5°, after which a solution of excess toluenesulfonyl chloride (TsCl) dissolved in 100 mL of cold (5°) dichloromethane was added to each flask. The temperature of each reaction was maintained at 5°-15° in a cold (-15°) ethylene glycol bath with swirling. Swirling was continued for about 20 min, or until reaction temperatures climbed by less than 3 °C/min without the aid of the cooling bath. The resulting reaction flasks were stoppered and stored in a -10° freezer overnight. The contents of these flasks were then poured over 100 g batches of cracked ice. Cold (5°) 6 *N* HCl was then added to each resulting mixture, with stirring, until the aqueous layers of these mixtures turned pH paper red ($pH \leq 1$). This operation melted much or most of the ice in each mixture. The resulting three-phase mixtures were separated into ice/aqueous and organic components, and the ice/aqueous layers were each extracted with 50 mL of cold (5°) dichloromethane. Corresponding dichloromethane extracts were combined with their respective organic reaction mixture components and each of the resulting mixtures was extracted three times with 150 mL each time of 6 *N* HCl. The resulting organic layers were each washed once with 150 mL of water, dried ($MgSO_4$), filtered, and concentrated (rotary evaporation using water aspirator). Residual solvents were removed from each of the resulting off-white solids overnight at reduced pressure (1 Torr). ^1H FT-NMR spectra (100 MHz, $CDCl_3$) of these solids were all consistent with pure α,ω-ditosylates

corresponding to target α,ω-dimethoxyalkanes. These ditosylates were used without further analysis or purification to carry out the subsequent reactions. To each of six 1000 mL three-necked reaction flasks was added, with swirling, 100 mL (2.47 eq) of methanol and 3.00 g (131 meq) of metallic sodium. Vigorous reactions ensued that resulted in complete dissolution of the sodium into clear solutions. The ditosylates (8.0 g each) were added into the six resulting sodium methoxide solutions, and stirring was initiated. After an apparent incubation time of 5-10 min, the resulting reaction mixtures foamed vigorously for ≈ 1 h, after which time they stabilized, yielding white precipitates under yellow solutions. These latter reaction mixtures were stirred at reflux overnight, cooled to room temperature, and partitioned between 100 mL of water and 100 mL of ether. The resulting organic layers were washed three times with 100 mL each time of water, dried ($MgSO_4$), filtered, and concentrated (rotary evaporation using water aspirator), yielding six yellow oils. These oils were then bulb-to-bulb (Kugelrohr) distilled yielding colorless oils. These latter oils were then purified by preparative gas chromatography as described previously for the lower-series diethers. All of the resulting purified higher-series diethers were at least 97% pure by GC analysis. Boiling points were estimated by assuming boiling points of diethers to be linearly related to the logs of their retention times and further assuming that diethers behave like straight-chain alkanes in this regard under the gas-chromatographic conditions outlined previously.[32] Linear-hydrocarbon standard mixtures obtained from Alltech Assoc., Inc. were used to calibrate the boiling point vs. log retention-time behaviors in our system for the column temperatures and flow rates at which these analyses were performed. All estimated boiling points were in reasonable agreement with literature values except for that of DME(6), for which no literature boiling point could be found, and of DME(12), for which the two literature values found[33,34] disagreed with each other by ≈ 100° when extrapolated to 760 Torr. ^1H FT-NMR spectra ($CDCl_3$) were consistent with pure

higher-series diethers. Final isolated yields and estimated and literature boiling points of these higher-series diethers are given in Table II.

Table II. Synthetic parameters for higher-series diether preparations.

	DME(6)	DME(7)	DME(8)	DME(9)	DME(10)	DME(12)
wt, g (meq) diol used	5.00(84.6)	5.00(75.6)	5.00(68.4)	5.00(62.4)	5.00(57.4)	5.00(49.4)
wt, g (meq) TsCl used	17.75(93.08)	15.86(83.21)	14.34(75.23)	13.09(68.66)	12.03(63.10)	10.37(54.39)
wt, g (meq) ditosylate	13.98(65.56)	8.43(38.3)	14.14(62.20)	14.41(61.50)	12.59(52.50)	10.50(41.10)
yield ditosylate	77.5%	50.6%	90.9%	98.6%	90.9%	83.3%
wt, g (meq) ditosylate used	8.00(28.1)	8.00(36.3)	8.00(35.2)	8.00(34.1)	8.00(33.2)	8.00(31.3)
wt, g (meq) diether	0.97(13)	1.52(19.0)	2.00(23.0)	1.76(18.7)	2.04(20.2)	1.25(10.9)
single step yield	47%	52.3%	65.2%	54.8%	60.7%	34.7%
overall isolated yield	37%	26.5%	59.3%	54.0%	55.2%	28.9%
estimated bp, °C (760 Torr)	184	207	223	243	261	295
lit. bp, °C (press., Torr)	none	201[a]	108-109(15)[b]	114-115(10)[c]	119(10)[d]	265-267(760)[e] 160(0.7)[f]

[a] Reference 35. [b] Reference 36. [c] Reference 37. [d] Reference 38. [e] Reference 33. [f] Reference 34.

2.1.5 Acetate Esters

Acetate esters were prepared by dissolving the corresponding phenols in excess pyridine, adding excess acetic anhydride, and stirring the resulting reaction mixtures for at least eight hours, followed by cold aqueous workup and simple (bulb-to-bulb Kugelrohr) distillation or recrystallization from hexane. The melting points or boiling points agreed with literature values (see Table III).

Table III. Melting and boiling points of substituted phenyl acetates.

Substituent	mp or bp (Torr), °C	lit. bp/mp	lit. ref.
3-chloro	70.5(2)	105-109 (15-16)	40
3-bromo	86.5(2)	142 (34)	41
3-cyano	60.0-60.5	58	41
4-cyano	57.0-58.0	56-57	40
4-nitro	78.0-79.5	79	41

2.2 Kinetics

Reactions were carried out by weighing polyether catalysts in 1 cm x 3 mL square cuvettes, pipetting 3 mL of amine/chlorobenzene stock solution (see Table IV for amine stock concentrations) into the same cuvettes, thermostating the resulting solutions for 0.5 h at 25°, injecting 30-40 μL of ester/chlorobenzene solution into each cuvette (see Table IV for ester concentrations), stoppering the cuvettes, shaking, and collecting absorbance vs. time data at fixed wavelength (see Table IV for wavelengths used). The

appearance of substituted phenol (product) was followed at the wavelength selected. Isosbestic points were obtained for all esters studied under the reaction conditions employed in these aminolyses. Absorbance data were generated by a Cary 118C spectrophotometer with a five-cell timed sample changer. The data thus collected were timed, formatted, and tagged with sample numbers (1-5) by a Varian 310 data interface. The resulting time-absorbance sample data were stored on an 8 inch floppy diskette by a Data General Nova 3 minicomputer. Interleaved data from five separate simultaneously reacting samples were separated and stored by this system. Pseudo-first-order rate constants (excess butylamine) were obtained by feeding the diskette data to a modified version of the program LSKINI developed by Delos Detar,[39] which fits absorbance vs. time data to the equation $A = A_\infty + (A_0 - A_\infty) \exp(-k_{obs}\, t)$, where A_∞, $A_0 - A_\infty$, and k_{obs} are iteratively optimized to achieve the best possible least-squares fit of this equation to the experimental data. LSKINI was executed on an IBM model 370/3033 or 370/3081 mainframe computer system. Catalysis kinetics were run with five different catalyst concentrations in five sample cuvettes reacting simultaneously. This protocol was triplicated for each catalyst/ester combination studied. All samples in a simultaneous run were made from the same butylamine stock solution. Uncatalyzed studies were done by running five samples of the same butylamine stock solution simultaneously after adding 30-40 μL of ester, and quintuplicating this protocol using different butylamine concentrations. Rate constants were extracted from LSKINI k_{obs} output data by exploiting the rate equation[23,25] $k_{obs} = k_0\,[\text{amine}]^2 + k_{cat}\,[\text{amine}]\,[\text{catalyst}]$. Values for k_0 with different esters were obtained from the slopes of plots of k_{obs}/[amine] vs. [amine] from noncatalytic experiments in which five different amine concentrations were studied. Values for k_{cat} with different polyether catalysts and a given ester were obtained from the slopes of plots of k_{obs}/[amine] vs. [catalyst]. Kinetic slopes and Hammett slopes were calculated using a simple linear-least-squares program running on

a Texas Instruments TI99/4A home computer. The k_{obs} values obtained by this method are listed in the Appendix. Pseudo-first-order rate constants for 766 reactions were measured in this study.

Table IV. Experimental kinetics conditions used in aminolysis of substituted phenyl acetates.

Substituent	Wavelength monitored, nm	[Amine], *M*	10^5 [Ester], *M*
3-chloro	293	0.15	130
3-bromo	293	0.15	120
3-cyano	297.5	0.15	25
4-cyano	293	0.06	120
4-nitro	320	0.04	8.1

RESULTS AND DISCUSSION

3.1 The Inverse Macrocyclic Effect

In 1980 Hogan and Gandour demonstrated[15] that polyether catalysis of the butylaminolysis of 4-nitrophenyl acetate shows an inverse macrocyclic effect when the reaction is carried out in chlorobenzene. Thus pentaglyme, GLM(6), shows about a two-fold catalytic activity enhancement over 18-crown-6, CRN(6), in this chemistry. Chao and Cram found[14] that the glymelike compound **1** thiolyzes the 4-nitrophenyl acetate ester of proline, **2**, about 30% faster than does the crownlike compound **3**, when the reaction is carried out in 20% CH_3CH_2OH/CH_2Cl_2. This latter reaction is accelerated by complexation of the conjugate acid of **2** to the polyether regions of thiols **1** and **3** prior to ester thiolysis of **2**. The dipolar tetrahedral intermediate, $T^{\pm}$, in aryl ester aminolysis and the conjugate acid of **2** both contain secondary ammonium ions. Secondary ammonium ion guests bind very poorly to crown ether hosts relative to primary ammonium ion guests.[42] Apparently glymes are better hosts for secondary ammonium ion guests than are crown ethers, at least when these guests are transition structures (i.e., kinetic rather than equilibrium macrocyclic effects are being measured). Thus, the kinetic inverse macrocyclic effect observed in aminolysis of aryl acetates carried out in chlorobenzene appears to have its origin in the fact that the rate-determining transition structure for this reaction is a secondary ammonium ion.

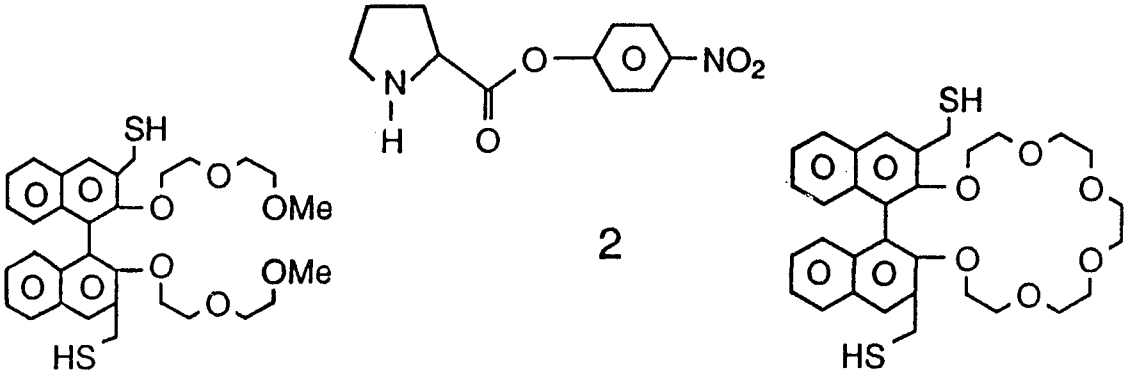

1 2 3

3.2 The Glyme-catalyzed Butylaminolysis Profile

Figure 2 and Table V profile the catalytic activities of the series of glymes, GLM(n), $2 \leq n \leq 9$, as catalysts in the butylaminolysis of 4-nitrophenyl acetate carried out in chlorobenzene. This profile shows a downward break at four oxygens. The catalytic profile above four oxygens extrapolates downward through the origin (intercept ± standard error = 0.008 ± 0.006 L^2 mol^{-2} s^{-1}). This shows that catalysis in the series having four or more oxygens is simply proportional to the concentration of glyme oxygens in solution and does not depend on the identity of the glyme species responsible for catalysis. It will be demonstrated later in this work that the breakpoint at GLM(4) corresponds to the size of the *catalytic segment* of a large glyme molecule responsible for optimum binding to the ammonium ion region of the rate-determining transition structure in the aminolysis reaction.

Table V. Catalytic power (k_{cat}) vs. oxygen-number profile for polyethers monoglyme through octaglyme.

Catalyst	Oxygens	10^2 *k*cat, M^{-2} s^{-1}	10^3 *k*cat/Oxy, M^{-2} s^{-1} oxy^{-1}
monoglyme	2	1.78 ± 0.03	8.9 ± 0.2
diglyme	3	17.4 ± 0.2	58.0 ± 0.7
triglyme	4	30.8 ± 0.3	77.0 ± 0.8
tetraglyme	5	38.1 ± 0.3	76.2 ± 0.6
pentaglyme	6	46.4 ± 0.3	77.3 ± 0.5
hexaglyme	7	53.5 ± 0.2	76.4 ± 0.3
heptaglyme	8	62.2 ± 0.8	78 ± 1
octaglyme	9	69.7 ± 0.5	77.4 ± 0.6

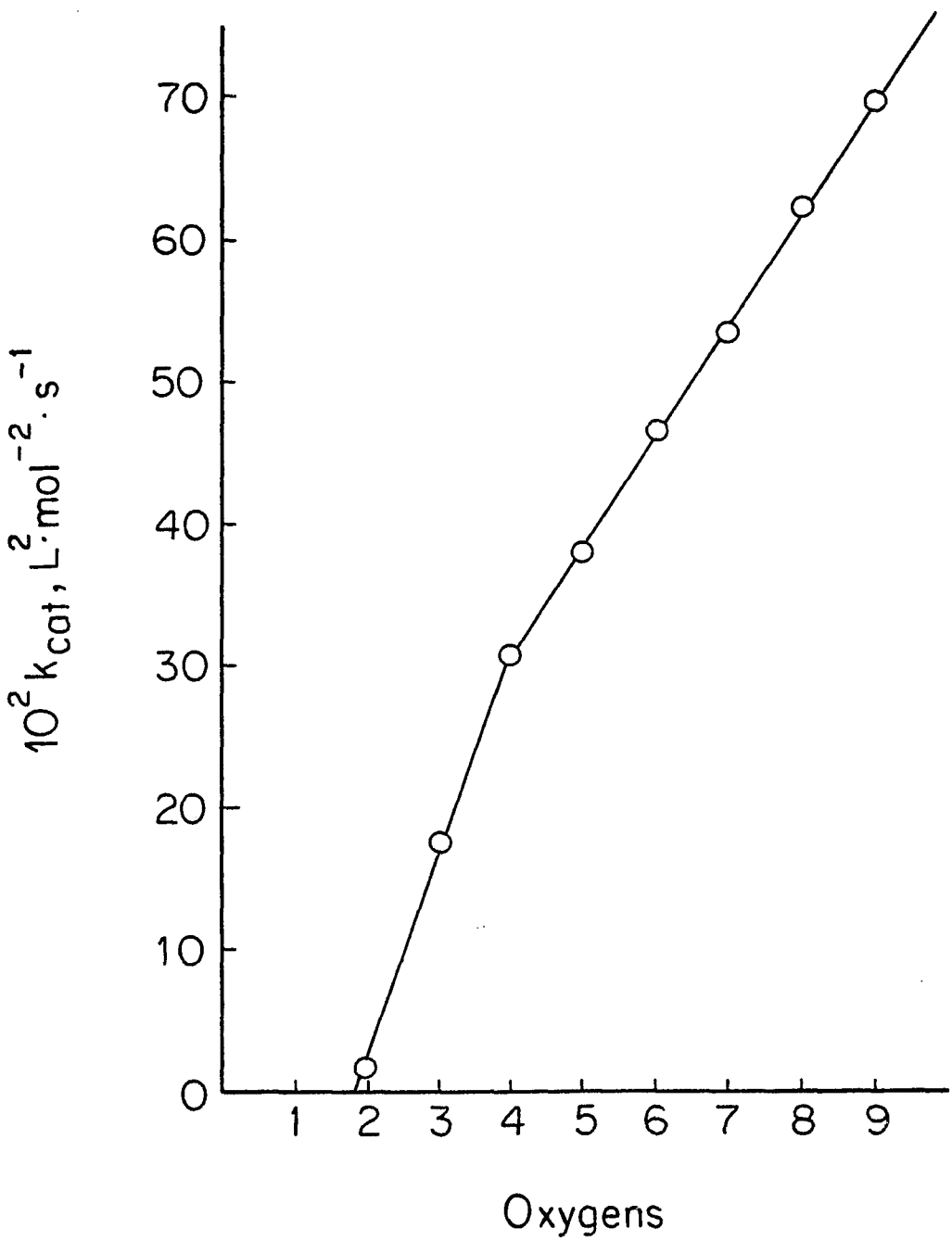

Figure 2. Plot of catalytic rate constant, k_{cat}, vs. the number of oxygens in the glyme catalyst molecule.

3.3 Kinetic Hammett Studies

3.3.1 Uncatalyzed Butylaminolysis Study

Values of k_o were determined for butylaminolysis of the esters listed in Table IV. A Hammett plot of log k_o vs. σ is shown in Figure 3. Values of σ^- were used instead of σ_p for the para-substituted esters studied (4-cyano and 4-nitro) in order to achieve the best possible correlation. Table VI lists substituent constants and uncatalyzed aminolysis rate constants. All substituent constants were obtained from Jaffe.[43] The ρ value obtained from this correlation is listed in Table VII.

Table VI. Uncatalyzed Hammett data from substituted phenyl acetate butylaminolysis kinetics.

Substituent	Sigma	$10^3\ k_o, M^{-2}\ s^{-1}$	Log k_o
3-chloro	0.37	1.08 ± 0.05	-2.97 ± 0.04
3-bromo	0.39	1.15 ± 0.03	-2.94 ± 0.02
3-cyano	0.68	4.7 ± 0.1	-2.32 ± 0.02
4-cyano	1.00	25.5 ± 0.4	-1.59 ± 0.01
4-nitro	1.27	65.1 ± 0.8[a]	-1.19 ± 0.01[a]

[a] Obtained from an analysis of the data presented in Ref. 44.

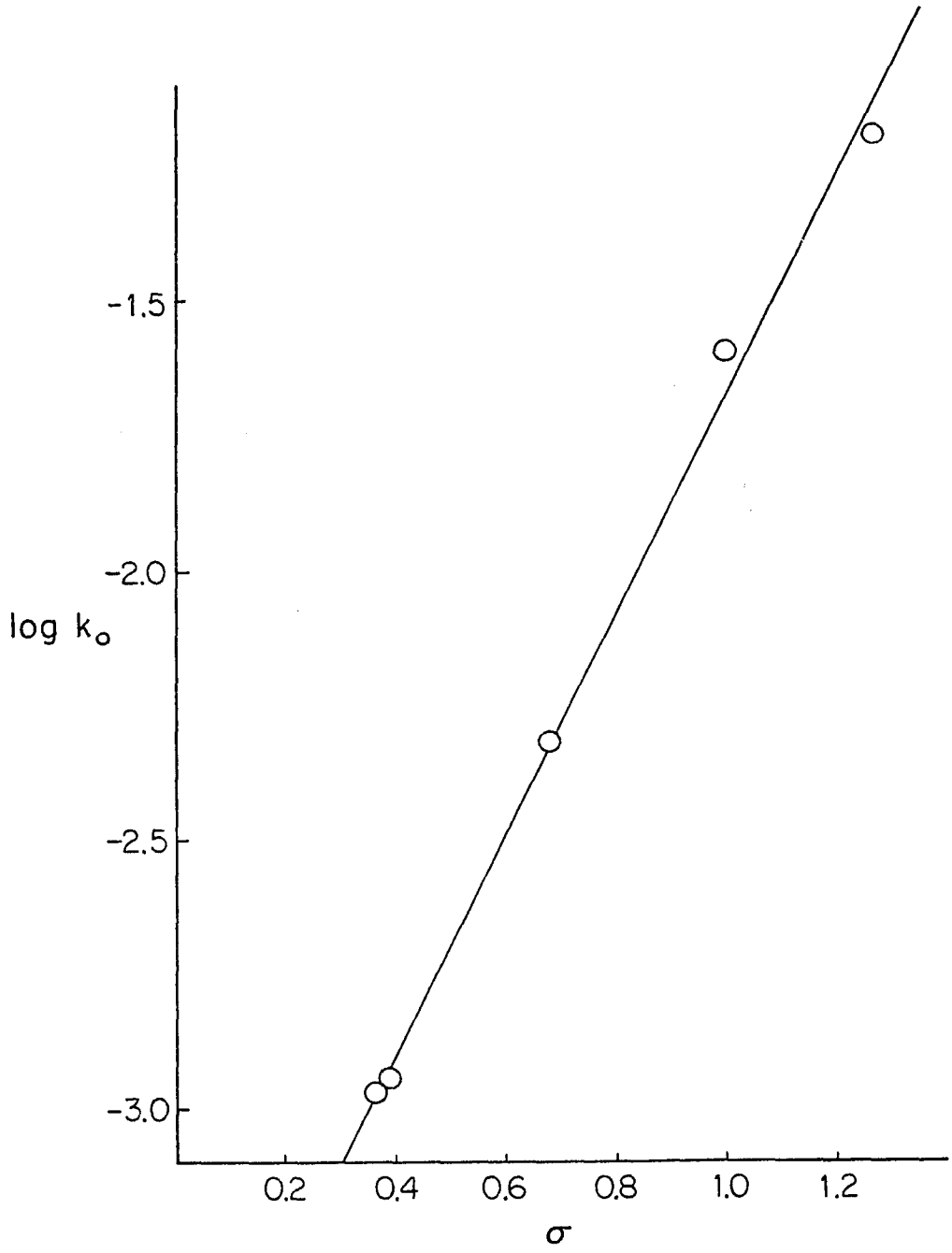

Figure 3. Uncatalyzed Hammett plot for the butylaminolysis of aryl acetates in chlorobenzene.

Table VII. Catalyzed and uncatalyzed Hammett rho values obtained from butylaminolysis rate-constant correlations.

Catalyst	Oxygens	Rho	$10^3\ k_{cat}$/Oxy, $M^{-2}\ s^{-1}\ oxy^{-1}$
none	- - - -	2.04 ± 0.08	- - - -
glyme	2	1.94 ± 0.09	8.9 ± 0.2
diglyme	3	2.16 ± 0.05	58 ± 1
triglyme	4	2.5 ± 0.1	77 ± 1
tetraglyme	5	2.4 ± 0.1	76 ± 1
octaglyme	9	2.4 ± 0.1	77.3 ± 0.5

3.3.2 Catalyzed Butylaminolysis Study: Bracketing the Transition Structure

Values of k_{cat} were determined for butylaminolysis of the esters listed in Table III catalyzed by GLM(n), n ϵ {2,3,4,5,9}. Table VIII lists log k_{cat} values resulting from these determinations. Figure 4 shows the Hammett plots corresponding to the catalyzed kinetic data in Table VIII. The same sigma values used for the uncatalyzed study were used for the catalyzed study. Rho values obtained from correlations of log k_{cat} vs. sigma are tabulated in Table VII. A plot of rho vs. oxygen number for the series of catalysts studied (Figure 5) shows an initial rise followed by a complete levelling off of this profile at four oxygens per molecule.

This behavior suggests that the catalytic structures responsible for binding to and facilitating the breakdown of $T^{\pm}$ push more and more negative charge onto the aryloxide nucleofuge (at the rate-determining transition structure) as the number of oxygens per glyme molecule increases until coordinative saturation is reached at four oxygens per

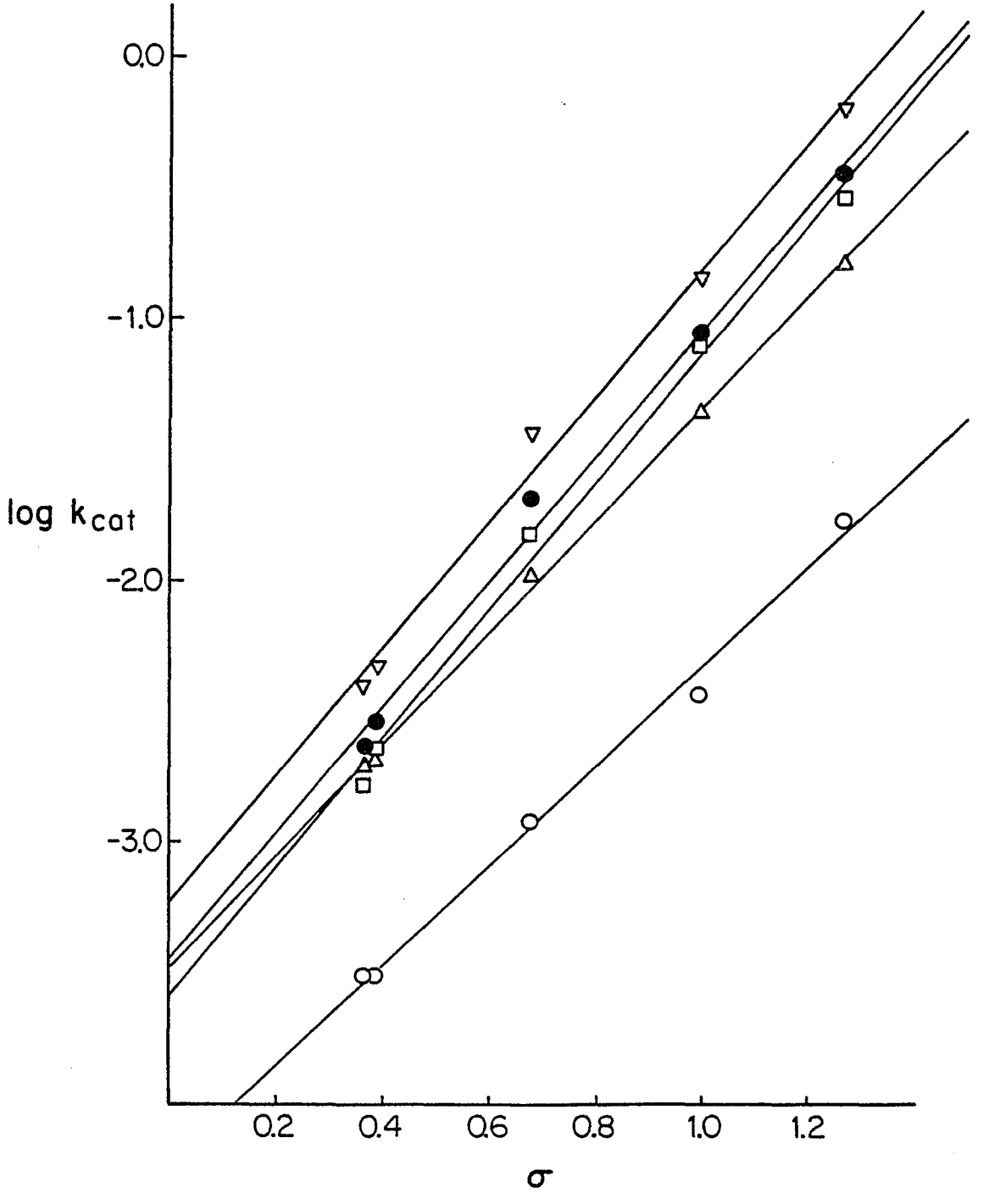

Figure 4. Catalyzed Hammett plots corresponding to data in Table VIII: (○) monoglyme (GLM(2)); (Δ) diglyme (GLM(3)); (□) triglyme (GLM(4)); (●) tetraglyme (GLM(5)); (∇) octaglyme (GLM(9)).

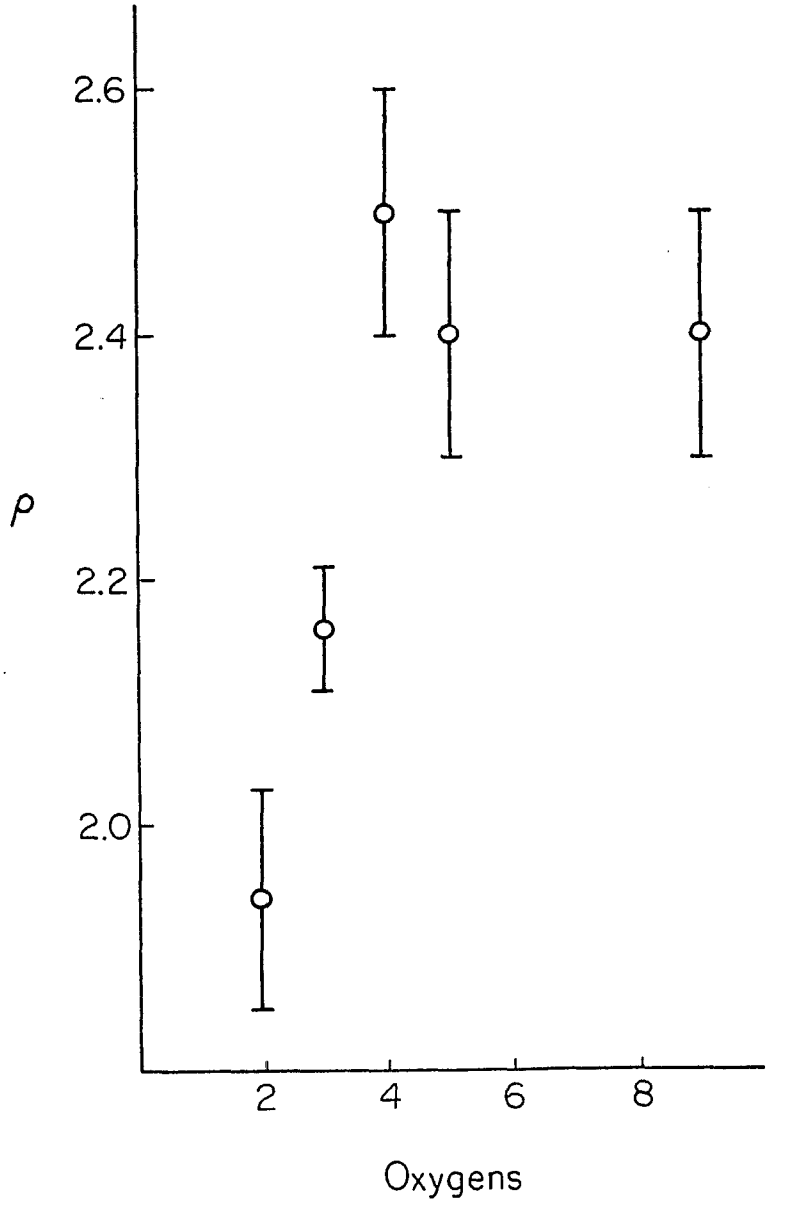

Figure 5. Plot of catalyzed (k_{cat}) Hammett rho value vs. oxygens per molecule of glyme catalysts. Rho values were obtained from the slopes of lines plotted in Figure 4. Error bars were derived from standard errors associated with linear-least-squares fits to the data.

glyme molecule. As the number of oxygens per catalyst molecule increases (in going from a two to a four oxygen catalyst) so does the value of rho, because rho in this reaction series is a measure of the relative amount of negative charge localized on the nucleofuge in the rate-determining transition structure. Catalysts having four or more oxygens all push the same amount of negative charge onto the nucleofuge in the rate-determining transition structure. This evidence taken in conjunction with the k_{cat} vs. oxygens per catalyst molecule profile discussed previously suggests that two through four oxygen catalysts bind to $T^{\pm}$ with different structures. Each of these structures has successively greater binding power and electron-pushing ability, whereas catalysts having four or more oxygens bind with the same structure to $T^{\pm}$.

Table VIII. Log k_{cat} values used in Hammett correlations.

Catalyst	3-chloro	3-bromo	3-cyano	4-cyano	4-nitro
none	-2.97 ± 0.04	-2.94 ± 0.02	-2.32 ± 0.02	-1.59 ± 0.01	-1.19 ± 0.01
GLM(2)	-3.5 ± 0.2	-3.5 ± 0.1	-2.91 ± 0.03	-2.42 ± 0.05	-1.75 ± 0.01
GLM(3)	-2.69 ± 0.04	-2.68 ± 0.04	-1.96 ± 0.02	-1.325 ± 0.007	-0.76 ± 0.01
GLM(4)	-2.77 ± 0.05	-2.63 ± 0.04	-1.80 ± 0.02	-1.09 ± 0.01	-0.511 ± 0.008
GLM(5)	-2.62 ± 0.03	-2.53 ± 0.04	-1.67 ± 0.01	-1.03 ± 0.02	-0.419 ± 0.006
GLM(9)	-2.39 ± 0.09	-2.31 ± 0.07	-1.42 ± 0.01	-0.82 ± 0.01	-0.157 ± 0.006

Assuming that basic polyether catalysts bind to the acidic ammonium ion part of $T^{\pm}$ and not to the basic nucleofuge part, polyethers must push charge onto the

nucleofuge indirectly. Because the nucleofuge is presumably expelled by the oxyanion of $T^{\pm}$ and the catalyst presumably interacts with the ammonium ion of $T^{\pm}$, a dipolar-stabilizing interaction must exist between the oxyanion piece of $T^{\pm}$ and the ammonium ion part of this zwitterion in aprotic media. This interaction is weakened by polyether binding, enabling the oxyanion to build up enough negative charge to stretch the bond tethering the nucleofuge to $T^{\pm}$ in the rate-determining transition structure. This in turn facilitates nucleofuge expulsion. The extent to which the polyether catalyst is able to raise the pK_a of the oxyanion of $T^{\pm}$ toward the development of a "naked"[7] oxyanion is reflected in the extent to which the oxyanion is then able to expel the aryloxide nucleofuge.

One mechanistic issue that has not yet been addressed here is whether butylamine preferentially preassociates with the polyether catalyst (or another butylamine molecule in the "uncatalyzed" mechanism) before attack of the resulting complex on the ester substrate, or alternatively the formation of uncomplexed $T^{\pm}$ is preferentially followed by binding to catalyst (or amine) preceding nucleofuge expulsion. The upper pathway in Scheme I shows butylaminolysis occurring without preassociation and the lower pathway shows butylaminolysis occurring with preassociation. There are currently no good experimental results available which allow resolution of this issue.

Scheme I

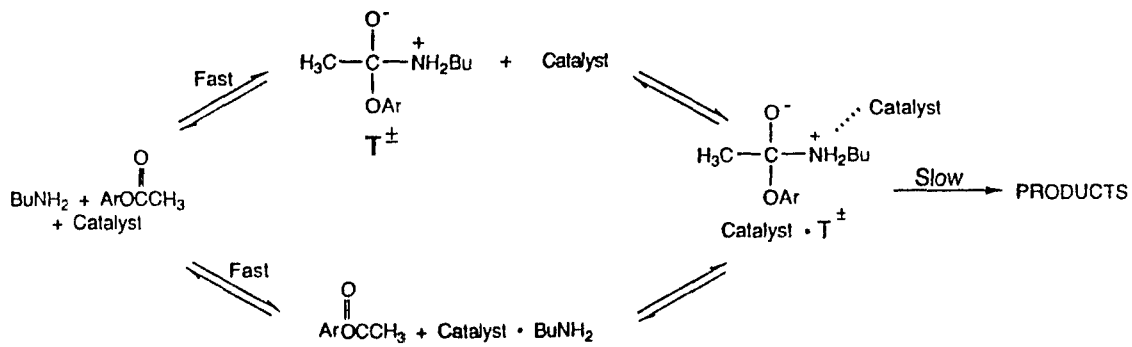

For the moment it will be shown that the rate-determining transition structure for butylaminolysis of aryl acetates in chlorobenzene occurs after formation of catalyst-complexed or amine-complexed $T^{\pm}$ regardless of whether or not preassociation occurs in this system. This fact may be demonstrated by an analysis of the effect of substituent and catalyst changes on the motion of the rate-determining transition structure in reaction-coordinate space. The Hammond postulate[46] and the experimental work of Jencks[47] involving acid-base catalysis can be summed up according to the mathematical treatment of Thornton[48] as follows: In a multidimensional reaction-coordinate space (two or more independent events or motions involved in a reaction pathway) any change in reagents or reaction conditions which perturbs the energetics of a reaction-coordinate surface moves the location of the transition structure away from regions of maximum stabilization (or toward regions of maximum destabilization) in the direction parallel to the tangent to the reaction path at the unperturbed transition-structure location ("Hammond" motion). Furthermore, such a change moves the transition structure in the opposite sense in all perpendicular directions ("anti-Hammond" motion). The implications of this behavior will now be examined first on the case in which butylaminolysis does not occur with preassociation, and next on the case in which preassociation does occur. It will be demonstrated that in both cases the catalytic Hammett behavior described above leads to the conclusion stated earlier, *viz.*, that catalyst-complexed or amine-complexed $T^{\pm}$ precedes the rate-determining transition structure.

Figure 6 models the reaction space for breakdown of $T^{\pm}$ assuming formation of $T^{\pm}$ precedes complexation to catalyst. The rate-determining transition structure cannot precede formation of $T^{\pm}$ (lower left corner) in this case because catalyst, ester, and amine fragments must *all* be involved in the rate-determining step in order to satisfy the observed third-order rate law. If the transition structure for the rate-determining step of

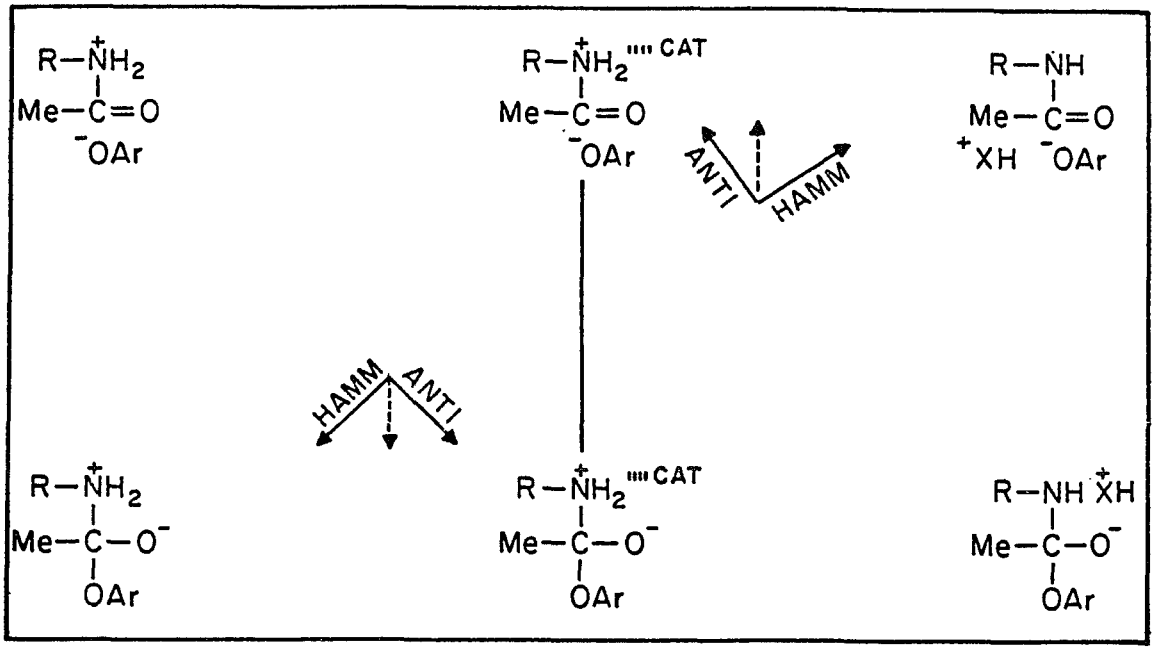

Figure 6. Reaction surface map of the breakdown of $T^{\pm}$ (lower left) to form product amide (upper right) assuming preassociation is not operative. Horizontal axis measures stretching of bond between nitrogen and abstractable proton, and vertical axis measures stretching of nucleofuge tethering bond. "X" is either some arbitrary base in the system or a bond between abstracted proton and expelled nucleofuge. "ANTI" shows qualitative direction of transition-structure motion along anti-Hammond diagonal, and "HAMM" shows qualitative Hammond motion. Locations of transition structures are arbitrary.

the reaction lies on the left side of the surface depicted in Figure 6, then an increase in the binding power of the catalyst should move the transition structure qualitatively from upper right to lower left (away from stabilization) along the "Hammond diagonal", because better catalysts should stabilize the catalyst-bound protonated amide (upper middle) region of the surface more than the unbound $T^{\pm}$ (lower left) region. Along the "anti-Hammond diagonal" the transition structure should then move from upper left toward lower middle (toward stabilization) with increasing catalyst binding power. The net result of these two motions should then bring the transition structure downward with increasing catalytic binding power. Because the lower part of the surface depicted in Figure 6 shows less negative charge on the nucleofuge segment than the upper part, a downward motion of the transition structure with catalyst improvement should occur with a *decrease* in the Hammett rho value as catalytic binding power *increases*, if the rate-determining transition structure lies on the *left* side of this surface. A similar analysis leads to the conclusion that if the rate-determining transition structure lies on the *right* side of the Figure 6 surface, then an *increase* in the binding power of a catalyst should lead to an upward motion of the transition structure, with a concurrent *increase* in the rho value. Figure 5 shows that the Hammett rho value increases with increasing catalytic binding power in this reaction class. Therefore if these aminolyses occur without preassociation then binding of catalyst to $T^{\pm}$ (the middle region of Figure 6) precedes the rate-determining transition structure (which must lie on the right side of Figure 6). To recapitulate: If nucleophilic attack of uncomplexed amine on ester is favored over attack of catalyst-complexed amine on ester then the rate-determining step for the total aminolysis occurs *after* catalyst binding, and involves breakdown of *bound* $T^{\pm}$.

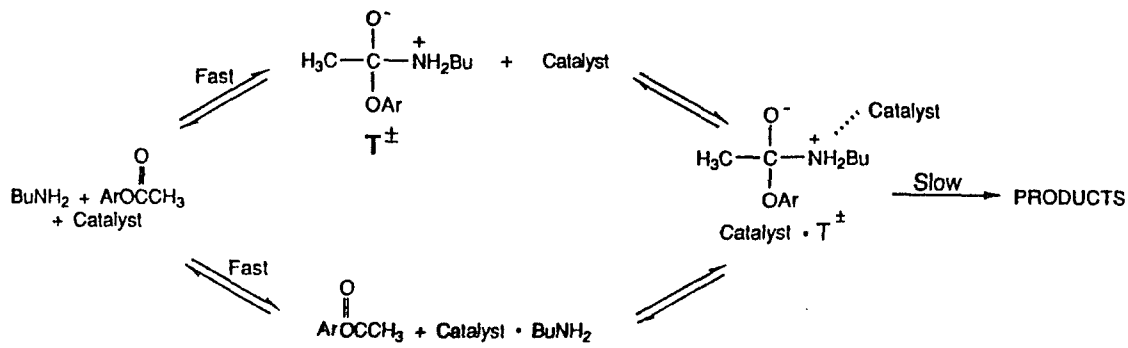

The logic necessary to demonstrate that the rate-determining step involves breakdown of bound $T^{\pm}$ even if nucleophilic attack does *not* precede catalyst binding (i.e., preassociation mechanism) is considerably simpler than the foregoing. In the preassociation mechanism only two possibilities need to be considered. Either a butylamine-catalyst complex attacks ester in the rate-determining step to form complexed $T^{\pm}$ which subsequently breaks down rapidly, or complexed $T^{\pm}$ forms quickly and breaks down slowly (i.e., the rate-determining step involves breakdown of bound $T^{\pm}$). The former possibility can be ruled out on the basis of the behavior of the rho value by using a Hammond[46] analysis (a one-dimensional Thornton analysis). Because catalyst should stabilize charged $T^{\pm}$ more than neutral butylamine a transition structure lying between catalyst-bound butylamine and catalyst-bound $T^{\pm}$ should move to an earlier point on this reaction path (toward the lesser stabilization) as catalytic binding power is increased. For such a transition structure to be rate-determining the rho value for the reaction would have to *decrease* with increasing catalytic binding power as the transition structure takes on more neutral ester character and less zwitterionic $T^{\pm}$ character (because $T^{\pm}$ presumably has more negative charge buildup on its nucleofuge segment than does free ester). This is contrary to what is experimentally observed. In summary, it can be seen that formation of complexed $T^{\pm}$ precedes the rate-determining transition structure by either a preassociative or nonpreassociative mechanism.

3.4 Butylaminolysis Catalyzed by Glymes: The Catalytic Segment

Figure 7 profiles the catalytic behavior of glymes in butylaminolysis discussed in section 3.2 except that catalytic activities have been presented on per-oxygen basis (see Table V). The behavior shown in Figure 7 parallels the Hammett behavior profiled in Figure 5. This shows that catalysis on a per-oxygen basis improves due to increased binding ability with increasing oxygens per molecule in the glyme series, up to triglyme (GLM(4)). Glymes larger than triglyme do not bind differently from triglyme to the rate-determining transition structure for the reaction. The catalytic activities of glymes larger than triglyme increase with oxygen number on a molar basis (as opposed to a per-oxygen basis) merely due to the fact that longer glymes present bigger targets for a $T^{\pm}$ encounter than shorter glymes. This behavior is purely statistical; it is indistinguishable from concentration behavior (hence the extrapolation of large glyme catalytic behavior through the origin in Figure 2). A 0.05 molar GLM(8) solution for example, would show exactly the same kinetic behavior as would the 0.10 molar solution of GLM(4), which would be obtained by cutting all of the GLM(8) molecules in half and adding H_2 across the freshly cut ends. In summary, it can be stated that glyme-catalyzed butylaminolysis in aprotic solvents is optimal with a four $-CH_2OCH_2-$ unit long catalytic segment. The nature of the binding of the rate-determining transition structure with this catalytic segment will be examined in greater detail throughout much of the remainder of this work.

Plotted with the polyether data in Figure 7 is the per-oxygen catalytic power of DME(12) in butylaminolysis. DME(12) is the largest of the α,ω-dimethoxyalkanes studied in this work; it has the greatest separation between terminal oxygens of any of the diethers studied here. The magnitude of its per-oxygen catalytic power suggests that it binds only one oxygen to the catalytic site in butylaminolysis, making it an adequate model for a single-oxygen polyether (on a per-oxygen basis). There are two reasons for

stating this. Primarily, the per-oxygen catalytic power of DME(12) is less than, but within error of, the catalytic power measured by Su and Watson[23] of tetrahydrofuran (a one-oxygen ether) in butylaminolysis carried out under conditions identical to those used here. Secondarily, examination of Figure 7 shows it to be a sigmoidal curve, and the data point for DME(12) appears to fall qualitatively where it belongs in this profile.

3.5 Methylbutylaminolysis Catalyzed by Glymes: The Modified-site Catalytic Segment

The leftmost four columns of entries in Table IX and the plot in Figure 8 profile the catalytic activities of glymes, GLM(n), $2 \leq n \leq 4$, in 4-nitrophenyl acetate N-methylbutylaminolysis. Figure 8 is a plot of the per-oxygen catalytic powers in this polyether series vs. catalyst oxygen number analogous to Figure 7 discussed under the previous topic.

Table IX. Catalytic power (k_{cat}) vs. oxygen-number profile for polyethers monoglyme through triglyme catalyzing methylbutylaminolysis and associated relative transition-structure stabilizations.

Catalyst	Oxygens	$10^3\ k_{cat}$, $M^{-2}\ s^{-1}$	$10^4\ k_{cat}/Oxy$, $M^{-2}\ s^{-1}\ oxy^{-1}$	k_{oxcat}/k^o_{oxcat}	$-\Delta\Delta G^{\ddagger}_{oxy}$, kcal $mol^{-1}\ oxy^{-1}$	$-\Delta\Delta G^{\ddagger}_{o}$, kcal mol^{-1}
GLM(2)	2	11.1 ± 0.5	56 ± 3	2.8 ± 0.3	0.60 ± 0.06	1.2 ± 0.1
GLM(3)	3	16.1 ± 0.3	54 ± 1	2.7 ± 0.2	0.58 ± 0.04	1.17 ± 0.08
GLM(4)	4	22 ± 1	55 ± 3	2.8 ± 0.3	0.60 ± 0.06	1.2 ± 0.1

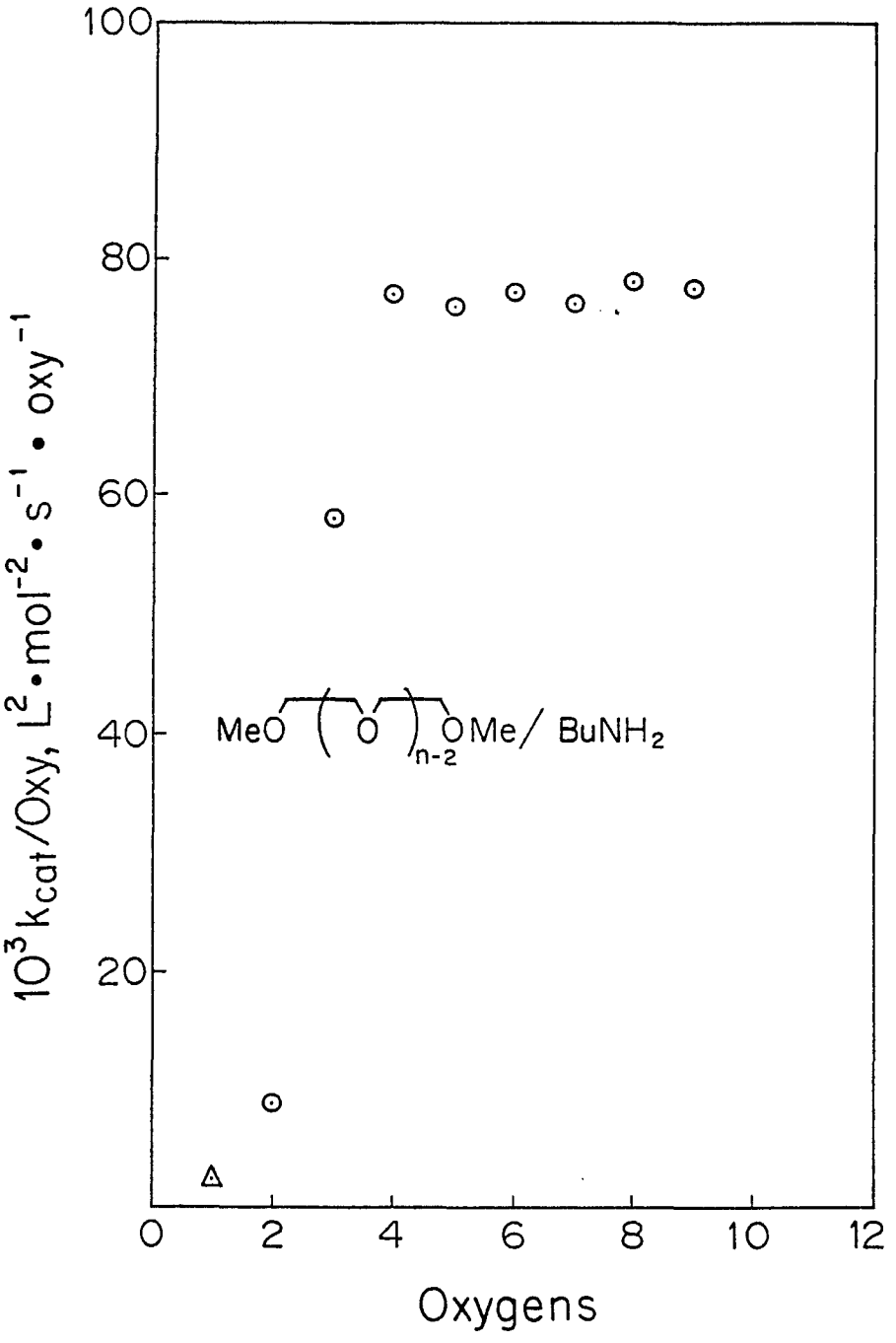

Figure 7. Plot of the per-oxygen catalytic rate constant, k_{cat}/Oxy, for butylaminolysis of 4-nitrophenyl acetate vs. the number of oxygens in the polyether catalyst molecule: (○) glymes; (Δ) DME(12).

Plotted with the polyether data is the per-oxygen catalytic power of DME(12) in methylbutylaminolysis. If this catalyst is unable to bind more than one oxygen to the catalytic site in butylaminolysis where there are two hydrogens available for binding, then it is probably reasonable to assume that the loss of a hydrogen at the binding site (replaced by a methyl group in methylbutylaminolysis) does not enhance the ability of the second oxygen in DME(12) to bind to the catalytic site. Further evidence for this assumption is presented under the topic following this one.

Figure 8 now appears to be a sigmoidal curve analogous to Figure 7 showing coordinative saturation of the rate-determining transition structure in methylbutylaminolysis by two polyether oxygens. Coordinative saturation (i.e., bifurcated hydrogen bonding[9]) of a one-hydrogen catalytic site by a two-oxygen catalytic segment and optimum binding by a four-oxygen catalytic segment to a two-hydrogen catalytic site has just been demonstrated. It is now tempting to suggest that each of the two hydrogens in the butylaminolysis catalytic site binds via bifurcated hydrogen bonds to two oxygens in polyethers having four or more oxygens (i.e., **4**). The possibility might still exist, however, that the central oxygens in the four-oxygen catalytic segments of large polyethers act merely as spacers and only the first and fourth oxygens in these segments actually bind one-on-one to the two catalytic site hydrogens in butylaminolysis (i.e., **5**). This possibility will be eliminated later in this work.

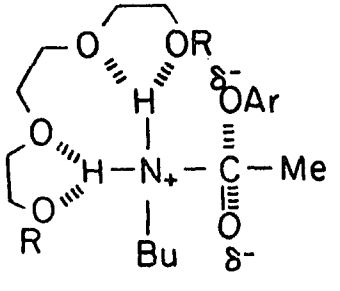

4

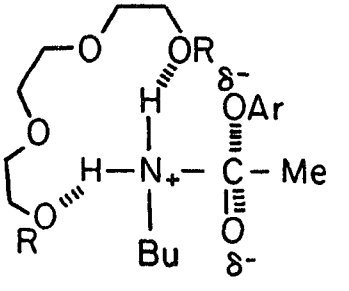

5

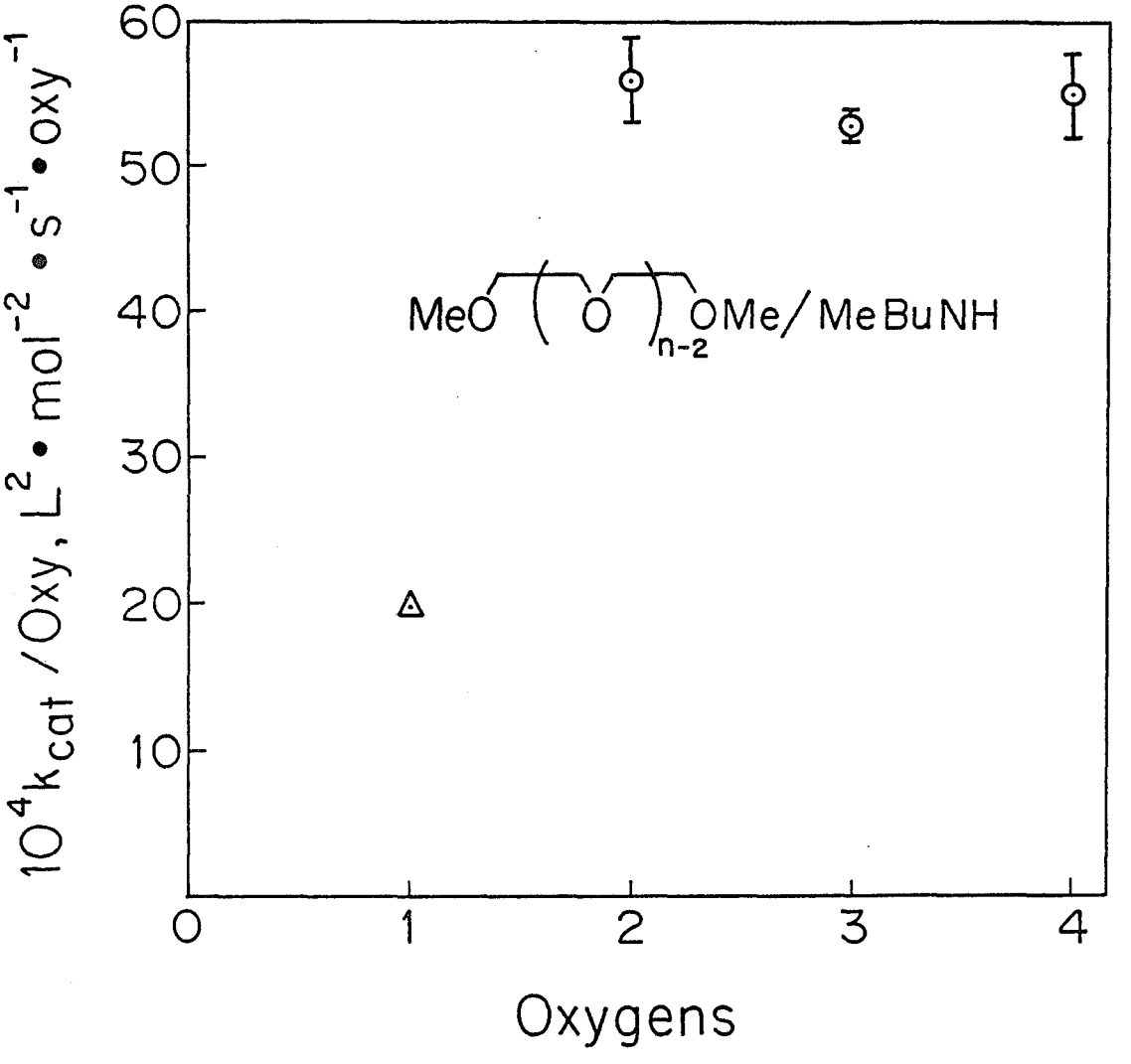

Figure 8. Plot of the per-oxygen catalytic rate constant, k_{cat}/Oxy, for the methylbutylaminolysis of 4-nitrophenyl acetate vs. the number of oxygens in the polyether catalyst molecule: (○) glymes; (Δ) DME(12).

3.6 Methylbutylaminolysis Catalyzed by Diethers: The Bifurcated Hydrogen Bond

The leftmost four columns of entries in Table X and the plot in Figure 9 profile the catalytic activities of α,ω-dimethoxyalkanes, DME(n), n ∈ {2,3,4,...,10,12}, in 4-nitrophenyl acetate methylbutylaminolysis. Figure 9 is a plot of the per-oxygen catalytic powers of the diether series vs. the number of methylenes between the terminal methoxy groups of the corresponding diethers.

The sharp activity drop which occurs with diethers larger than 1,2-dimethoxyethane is probably due to entropic difficulties faced by the system when longer diether catalysts attempt to form the larger rings necessary to give bifurcated hydrogen bonding to the single available hydrogen at the catalytic site. Some small amount of bifurcated hydrogen bonding may be occurring in diethers having up to 5 methylenes since a break is observed between DME(5) and DME(6). DME(5) has to form an eight-membered ring with the catalytic-site hydrogen in order to bifurcate bonding to the hydrogen. In view of the well-known difficulties reacting systems have forming rings having more than eight members,[49] higher-series diethers would not be expected to show measurable amounts of bifurcated hydrogen bonding. Figure 9 also demonstrates that DME(6) and higher diethers, including DME(12), can be treated like two noninteracting single-oxygen ether molecules with respect to catalytic activity in this system.

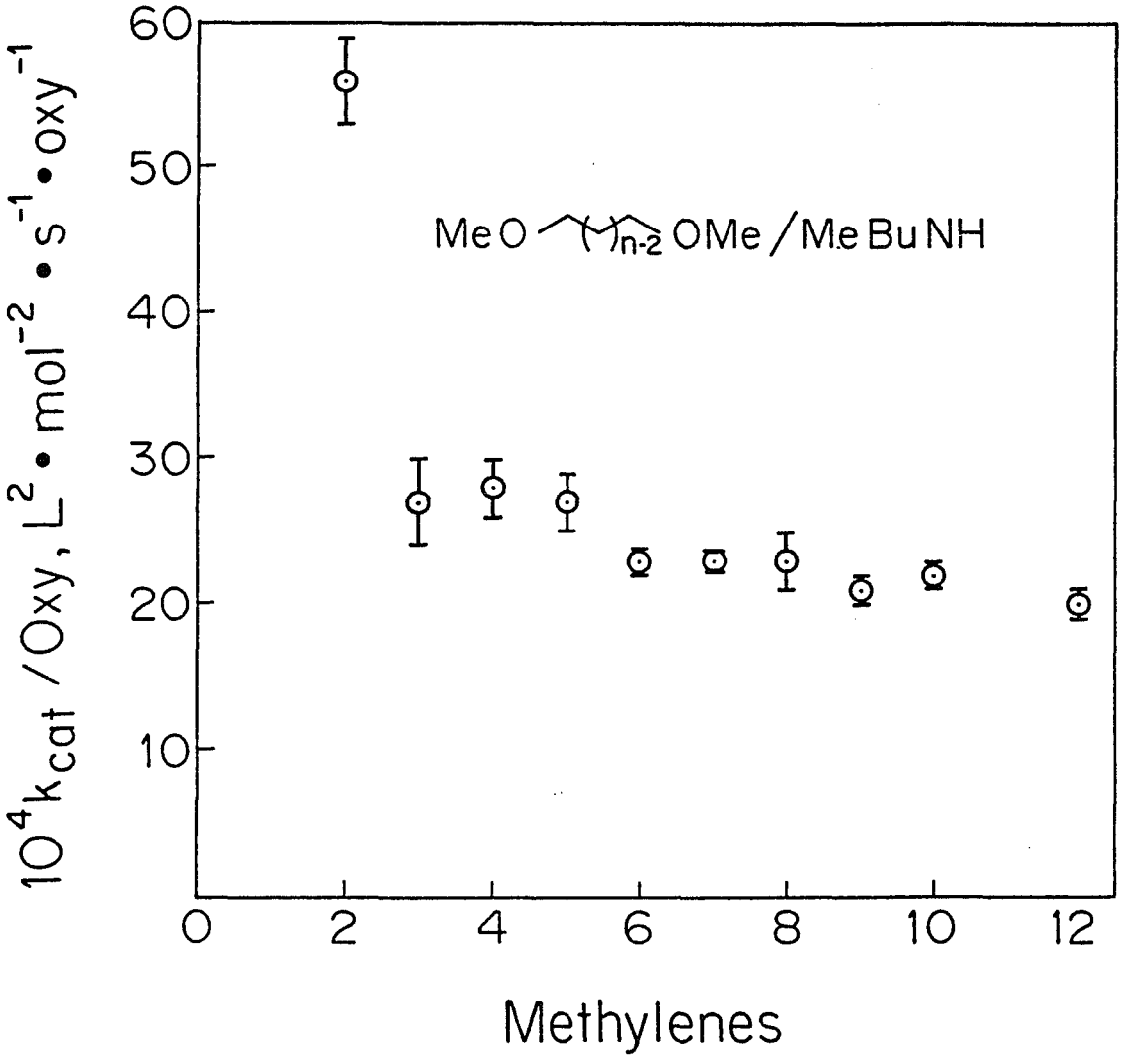

Figure 9. Plot of the per-oxygen catalytic rate constant, k_{cat}/Oxy, for the methylbutylaminolysis of 4-nitrophenyl acetate vs. the number of methylene groups in the α,ω-dimethoxyalkane catalyst molecule.

Table X. Catalytic power (k_{cat}) vs. internal methylene number profile for diethers 1,2-dimethoxyethane through 1,12-dimethoxydodecane catalyzing methylbutylaminolysis and associated relative transition-structure stabilizations.

Catalyst	Methylenes	$10^4\ k_{cat}$, $M^{-2}s^{-1}$	$10^4\ k_{cat}$/Oxy, $M^{-2}s^{-1}\ oxy^{-1}$	k_{oxcat}/k^{o}_{oxcat}	$-\Delta\Delta G^{\ddagger}_{oxy}$, kcal $mol^{-1}\ oxy^{-1}$	$-\Delta\Delta G^{\ddagger}_{o}$, kcal mol^{-1}
DME(2)	2	111 ± 5	56 ± 3	2.8 ± 0.3	0.61 ± 0.06	1.2 ± 0.1
DME(3)	3	54 ± 5	27 ± 3	1.4 ± 0.2	0.18 ± 0.09	-
DME(4)	4	56 ± 3	28 ± 2	1.4 ± 0.2	0.20 ± 0.07	-
DME(5)	5	53 ± 4	27 ± 2	1.4 ± 0.2	0.18 ± 0.09	-
DME(6)	6	46 ± 2	23 ± 1	1.2 ± 0.1	0.08 ± 0.09	0.08 ± 0.09
DME(7)	7	46.2 ± 0.9	23.1 ± 0.5	1.16 ± 0.09	0.09 ± 0.04	0.09 ± 0.04
DME(8)	8	46 ± 3	23 ± 2	1.2 ± 0.2	0.08 ± 0.08	0.08 ± 0.08
DME(9)	9	42 ± 1	21 ± 1	1.1 ± 0.1	0.03 ± 0.06	0.03 ± 0.06
DME(10)	10	44 ± 2	22 ± 1	1.1 ± 0.1	0.06 ± 0.06	0.06 ± 0.06
DME(12)	12	40 ± 2	20 ± 1	1.0 ± 0.1	0.00 ± 0.06	0.00 ± 0.06

3.7 Butylaminolysis Catalyzed by Diethers: The Catalytic Bridge

The leftmost four columns of entries in Table XI and the plot in Figure 10 profile the catalytic activities of α,ω-dimethoxyalkanes, DME(n), n ∈ {2,3,4,...,10,12}, in 4-nitrophenyl acetate butylaminolysis. Figure 10 is a plot of per-oxygen catalytic power vs. methylene number for the diether catalyst series, analogous to Figure 9 described under the previous topic. Figure 10 shows strong catalytic activity for DME(2), which suggests the same strong bifurcation in butylaminolysis by DME(2) as Figure 9

suggests in methybutylaminolysis, along with some possible weak bifurcation in the lower-series diethers. Figure 10 differs from Figure 9 in the catalytic behavior it shows in the higher-series diethers.

Butylaminolysis shows some vinculoselection[50] centered around the 9 methylene region that has to involve both hydrogens at the catalytic site because this activity does not appear with catalytic sites containing only one hydrogen (methylbutylaminolysis). Thus DME(8) and DME(10) show substantial amounts of bridging between the two catalytic site hydrogens in butylaminolysis, presumably via one-to-one hydrogen bonds formed between the two catalytic-site (ammonium) hydrogens and the two oxygens in the diether molecule[51] involved in catalysis at a given site. Interestingly, the center point of the activity region in the higher-series diethers corresponds to the diether (DME(9)) which would result if triglyme (GLM(4)) were to have both of its central oxygens replaced by methylene groups. This result suggests that the terminal oxygens in GLM(4) are well placed for bridging between the two ammonium hydrogens at the butylaminolysis catalytic site. GLM(4) shows about 14 times the per-oxygen catalytic activity or 28 times the overall catalytic activity in butylaminolysis that DME(8) and DME(10) show, however, which supports the idea that the central oxygens in GLM(4) are also involved in binding. Surprisingly, DME(9) itself shows very little bridging while the diethers to either side of it show a significant amount of bridging. Apparently DME(9) has some built-in conformational problems which put its oxygens into configurations unsuitable for bridging to the two ammonium hydrogens in butylaminolysis, although the exact nature of this problem is unclear.

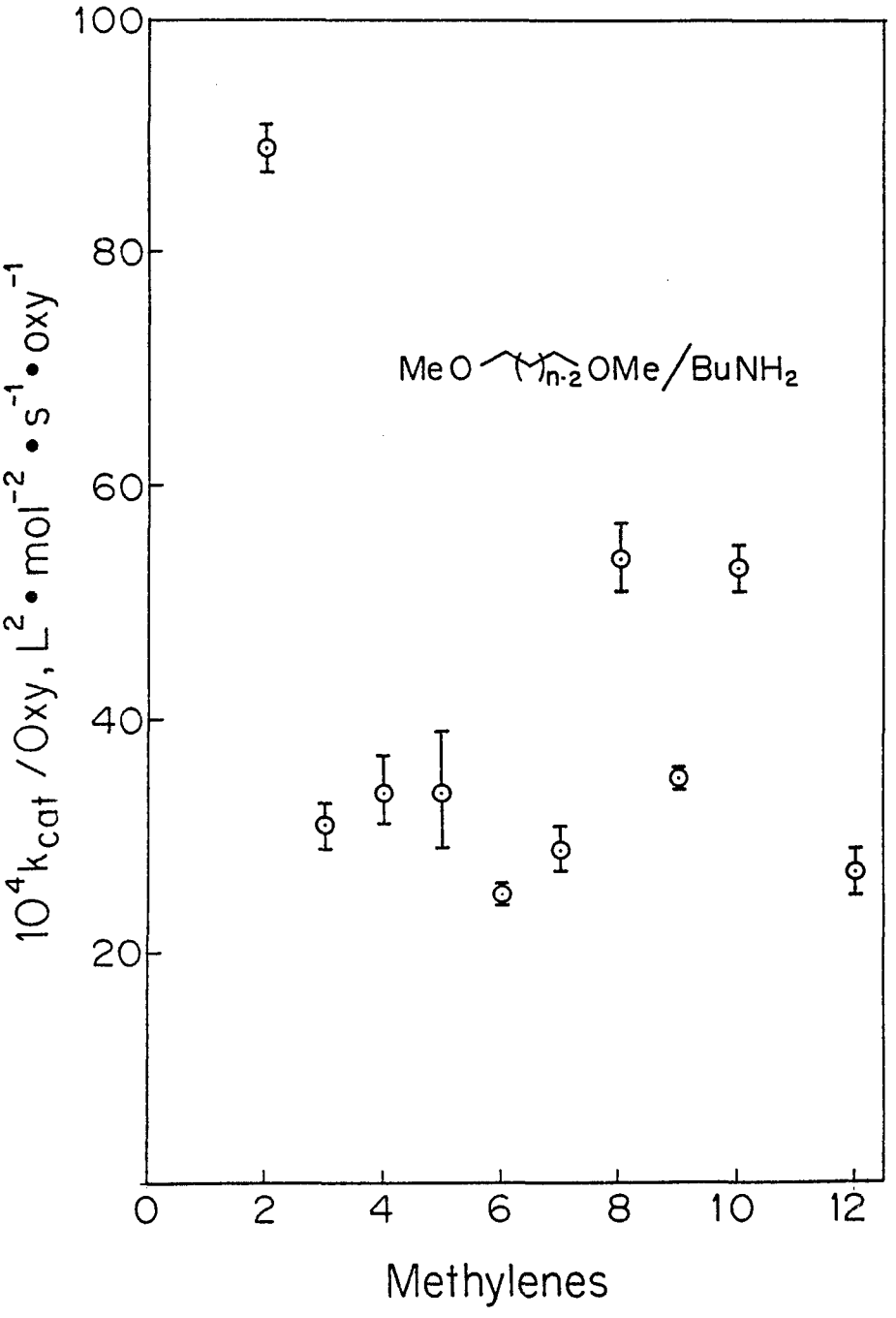

Figure 10. Plot of the per-oxygen catalytic rate constant, k_{cat}/Oxy, for butylaminolysis of 4-nitrophenyl acetate vs. the number of methylene groups in the α,ω-dimethoxyalkane catalyst molecule.

Table XI. Catalytic power (k_{cat}) vs. internal methylene number profile for diethers 1,2-dimethoxyethane through 1,12-dimethoxydodecane catalyzing butylaminolysis and associated relative transition-structure stabilizations.

Catalyst	Methylenes	$10^4\ k_{cat}$, $M^{-2}\ s^{-1}$	$10^4\ k_{cat}/Oxy$, $M^{-2}\ s^{-1}\ oxy^{-1}$	k_{oxcat}/k^{o}_{oxcat}	$-\Delta\Delta G^{\ddagger}_{oxy}$, kcal $mol^{-1}\ oxy^{-1}$	$-\Delta\Delta G^{\ddagger}_{o}$, kcal mol^{-1}
DME(2)	2	178 ± 3	89 ± 2	3.3 ± 0.2	0.71 ± 0.04	1.41 ± 0.07
DME(3)	3	62 ± 3	31 ± 2	1.1 ± 0.1	0.08 ± 0.06	-
DME(4)	4	68 ± 5	34 ± 3	1.3 ± 0.3	0.14 ± 0.07	-
DME(5)	5	67 ± 9	34 ± 5	1.3 ± 0.4	0.1 ± 0.1	-
DME(6)	6	50 ± 2	25 ± 1	0.96 ± 0.01	-0.05 ± 0.05	-0.05 ± 0.05
DME(7)	7	57 ± 4	29 ± 2	1.1 ± 0.1	0.04 ± 0.06	-
DME(8)	8	108 ± 6	54 ± 3	2.0 ± 0.2	0.41 ± 0.05	-
DME(9)	9	69 ± 2	35 ± 1	1.30 ± 0.09	0.15 ± 0.04	-
DME(10)	10	105 ± 3	53 ± 2	2.0 ± 0.2	0.40 ± 0.04	-
DME(12)	12	53 ± 1	27 ± 1	0.00 ± 0.08	0.00 ± 0.01	0.00 ± 0.01

The diether DME(5), which can be used to model diglyme (GLM(3)) with its central oxygen replaced by methylene, does not appear to be very well suited for bridging between the ammonium hydrogens in butylaminolysis from the data plotted in Figure 10. GLM(3) shows about a 17-fold per-oxygen catalytic enhancement over DME(5) in butylaminolysis, however, which is similar to the enhancement exhibited by GLM(4) over DME(8) and DME(10). Also the per-oxygen catalytic power of GLM(3) is over six times that of GLM(2) in butylaminolysis, which is far too high for GLM(3) to be catalyzing by binding to only one of the two ammonium hydrogens at the

butylaminolysis catalytic site. Therefore GLM(3) appears to bind all three of its oxygens to the catalytic site in butylaminolysis, and binds to (bridges) both ammonium hydrogens, albeit imperfectly.

The fact that GLM(4) shows a 30% better per-oxygen catalytic ability than GLM(3) in butylaminolysis suggests that GLM(4) binds all four oxygens to the two ammonium hydrogens at the catalytic site, and that it bridges these catalytic site hydrogens more effectively than GLM(3). Indeed, bridging is probably near optimal in GLM(4) given the higher-series diether behavior plotted in Figure 10, suggesting that GLM(4) catalysis of butylaminolysis emulates either the "lock-and-key" or "induced-fit"[52] behavior found in enzymes. It appears that GLM(4) catalyzes butylaminolysis by bridging together two pairs of bifurcating oxygens to form a doubly-bifurcated hydrogen-bonded transition-structure complex (**4**, R = Me).

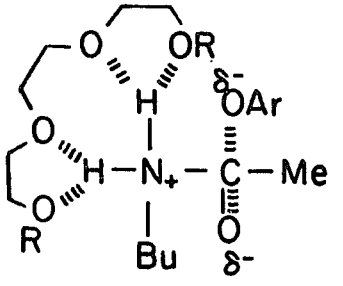

4

The last issue to be discussed here concerns the validity of the assumption made earlier that DME(12) binds only one oxygen to the catalytic site in butylaminolysis (does not bridge). The complexity of the profile shown in Figure 10 does not make it obvious that DME(6) and DME(12) lie on the catalytic-activity baseline of the butylaminolysis profile (i.e., exhibit no bifurcation or bridging). However, the discussion in the preceding paragraph demonstrates that the catalytic activity of DME(12) lies on the baseline of the methylbutylaminolysis profile. The DME(2):DME(12) catalytic-activity

ratios for butylaminolysis and methylbutylaminolysis were therefore calculated on the assumption that the bifurcation-to-baseline (single oxygen hydrogen bonding) catalytic-activity ratios should be similar in both reaction classes. The DME(2):DME(12) catalytic-activity ratios for butylaminolysis and methylbutylaminolysis (3.3 ± 0.2 and 2.8 ± 0.3) are nearly the same. Thus DME(12) catalytic data can be used to model single hydrogen-bond catalysis in both butylaminolysis and methylbutylaminolysis by dividing observed DME(12) catalytic activities in half to compensate statistically for the presence of the second oxygen.

3.8 Energy Calculations

3.8.1 Transition-structure Stabilizations

The rightmost three columns of table entries in Tables IX-XII involve calculations of relative transition-structure stabilizations on a per-oxygen basis and, where only one catalytic structure is presumed to be operative, on a per-structure basis. These transition-structure stabilizations were calculated relative to the stabilizations that would be observed in hypothetical reactions in which each catalytic oxygen is allowed to bond to its appropriate region of the catalytic site with only a single simple hydrogen bond worth of energy, and oxygens not involved in catalytic-site binding are ignored.

The first step taken in carrying out catalytic energy calculations was to determine per-oxygen relative catalytic activities for all catalysts studied in each reaction protocol (butylaminolysis and methylbutylaminolysis). Each per-oxygen relative catalytic activity was calculated by dividing the per-oxygen catalytic rate constant measured for a given catalyst in a given reaction protocol, k_{oxcat}, by the per-oxygen catalytic rate constant measured for DME(12) in the same reaction protocol, k^{o}_{oxcat}. Tables IX-XII list calculated per-oxygen relative catalytic activities under the heading k_{oxcat}/k^{o}_{oxcat}. The k^{o}_{oxcat} values used for butylaminolysis and methylbutylaminolysis protocols, 0.0027

M^{-2} s^{-1} oxy^{-1} and 0.0020 M^{-2} s^{-1} oxy^{-1}, respectively, are found in Table XI and Table X, respectively. DME(12) was chosen to model the reference catalyst, for reasons outlined under the previous topic. Per-oxygen relative catalytic activities were converted to per-oxygen relative transition-structure stabilizations, $-\Delta\Delta G^{\ddagger}_{oxy}$, using the formula $-\Delta\Delta G^{\ddagger}_{oxy} = RT \ln (k_{oxcat}/k^{o}_{oxcat})$. In cases where only a single catalytic structure was presumed to be operative, per-oxygen relative transition-structure stabilizations were converted to total (per-structure) relative transition-structure stabilizations, $-\Delta\Delta G^{\ddagger}_{o}$, by multiplying calculated $-\Delta\Delta G^{\ddagger}_{oxy}$ values by the number of catalyst oxygens presumed to bind to the catalytic site for each catalyst-reaction protocol combination. As an example of this, the catalyst GLM(3) was presumed to bind three oxygens to the catalytic site in butylaminolysis, but only two to the methylbutylaminolysis catalytic site. Calculated values for $-\Delta\Delta G^{\ddagger}_{oxy}$ and $-\Delta\Delta G^{\ddagger}_{o}$ are given in Tables IX-XII.

Table XII. Catalytic power (k_{cat}) vs. oxygen-number profile for polyethers monoglyme through octaglyme catalyzing butylaminolysis and associated relative transition-structure stabilizations.

Catalyst	Oxygens	10^3 k_{cat}, M^{-2} s^{-1}	10^3 k_{cat}/Oxy, M^{-2} s^{-1} oxy^{-1}	k_{oxcat}/k^{o}_{oxcat}	$-\Delta\Delta G^{\ddagger}_{oxy}$, kcal mol^{-1} oxy^{-1}	$-\Delta\Delta G^{\ddagger}_{o}$, kcal mol^{-1}
GLM(2)	2	17.8 ± 0.3	8.9 ± 0.2	3.3 ± 0.2	0.71 ± 0.04	1.41 ± 0.07
GLM(3)	3	174 ± 2	58.0 ± 0.7	21 ± 1	1.82 ± 0.03	5.45 ± 0.09
GLM(4)	4	308 ± 3	77.0 ± 0.8	29 ± 1	1.99 ± 0.03	7.9 ± 0.1
GLM(5)	5	381 ± 3	76.2 ± 0.6	28 ± 1	1.98 ± 0.03	7.9 ± 0.1
GLM(6)	6	464 ± 3	77.3 ± 0.5	29 ± 1	1.99 ± 0.03	8.0 ± 0.1
GLM(7)	7	535 ± 2	76.4 ± 0.3	28 ± 1	1.98 ± 0.02	7.9 ± 0.1
GLM(8)	8	622 ± 8	78 ± 1	29 ± 1	1.99 ± 0.03	8.0 ± 0.1
GLM(9)	9	697 ± 5	77.4 ± 0.6	29 ± 1	1.99 ± 0.03	8.0 ± 0.1

3.8.2 Binding Energies

Bifurcation and bridging energies in this system were calculated from the total relative transition-structure stabilizations listed in Tables IX-XII. Bifurcation energies were taken directly from $-\Delta\Delta G_0^{\ddagger}$ values for GLM(2) in butylaminolysis and for GLM(n), $2 \leq n \leq 4$, in methylbutylaminolysis. Since $-\Delta\Delta G_0^{\ddagger}$ values tabulated already give energy differences for transition-structure stabilizations due to actual catalytic binding vs. hypothetical binding involving all active oxygens as single simple hydrogen-bond accepters, any catalyst-reaction protocol combination that yields exactly one bifurcated hydrogen bond (with two catalytic oxygens) per catalytic site should give a bifurcation energy identical to its $-\Delta\Delta G_0^{\ddagger}$ value. In the butylaminolysis reaction protocol DME(2) (the same catalyst as GLM(2)) satisfies this criterion, and in the methylbutylaminolysis protocol DME(2), DME(3), and DME(4) all satisfy this criterion. The bifurcation energy in methylbutylaminolysis seems to be about 1.2 kcal mol^{-1}. In butylaminolysis this energy appears to be about 1.4 kcal mol^{-1}. These energies are in agreement with theoretical (gas-phase) oxygen-donor bifurcation energies of 1-2 kcal/mol calculated for water trimers by Newton and coworkers.[53] The apparent difference between the calculated bifurcation energies in butylaminolysis and methybutylaminolysis may not be significant. A bridging energy for butylaminolysis was calculated by comparing GLM(4) catalysis to two independent bifurcations. Two bifurcations give a total $-\Delta\Delta G_0^{\ddagger}$ value of 2.8 kcal mol^{-1} in butylaminolysis, and the $-\Delta\Delta G_0^{\ddagger}$ value for GLM(4) in this protocol is 7.9 kcal mol^{-1}. Thus it appears that bifurcation contributes about 1.4 kcal mol^{-1} and that bridging of pairs of binding oxygens between ammonium hydrogens contributes about 5.1 kcal mol^{-1} to transition structure stabilization in butylaminolysis.

3.9 Other Mechanistic Considerations

One ammonium hydrogen and its aryloxide nucleofuge must be lost from $T^{\pm}$ to yield product amide. As discussed previously, the fact that the rate-determining step in aminolysis changes from formation of $T^{\pm}$ in protic solvents to breakdown of $T^{\pm}$ in aprotic solvents with a concurrent reaction-rate diminution of several orders of magnitude, seems to suggest that breakdown of $T^{\pm}$ yields an unstable intermediate in aprotic solvents which is avoided in protic solvents. Tetrahexylammonium benzoate (THAB) in aprotic solvents switches the system to protic solvent chemistry, which suggests that the culprit here (the unstable intermediate) is an N-protonated amide, which is avoided with THAB, since THAB is capable of deprotonating $T^{\pm}$ before aryloxide expulsion, whereas aprotic solvents and less powerful base catalysts are not.[26] This reasoning is corroborated by the observation that a wide variety of nitrogen and oxygen bases in various aprotic solvents catalyze a wide range of aminolyses strictly in accord with their (the nitrogen and oxygen bases) hydrogen-bonding abilities in systems showing aprotic solvent chemistry. These bases show no correlation between their basicities and their catalytic activities in this chemistry.[23,24] If proton loss from $T^{\pm}$ precedes aryloxide expulsion in aprotic media it has to be rate-determining, because the subsequent aryloxide expulsion by an oxyanion is energetically favorable (aryloxide anions should have lower pK_a values than amino alcohol oxyanions). Furthermore, as has just been discussed, the use of base catalysts strong enough to deprotonate $T^{\pm}$ in aprotic media (i.e., THAB) changes the rate-determining step from decomposition of $T^{\pm}$ to formation of $T^{\pm}$, giving rise to second-order (rather than third-order) kinetics. This rate-determining step change would be impossible if deprotonation of $T^{\pm}$ occurred in a fast step. It is difficult to believe that the speed of rate-determining proton abstraction by bases shows no correlation with base strength. If aryloxide expulsion from $T^{\pm}$ precedes proton abstraction to yield an N-protonated amide, however, hydrogen bonding by base

catalysts to the ammonium hydrogens should stabilize the rate-determining transition structure involved in aryloxide expulsion. This should speed up the reaction rate, and the hydrogen bonding should also stabilize the N-protonated amide intermediate following the rate-determining transition structure. Furthermore, because hydrogen bonding (not proton abstraction) is responsible for transition-structure stabilization in such a scenario, catalysis in this case should correlate with hydrogen-bonding ability and not base strength, which is what is experimentally observed. N-protonated amides, although unstable, are involved in preference to O-protonated amides, in certain acid-catalyzed NH proton exchanges in amides.[54]

In spite of all of the foregoing, the perception still exists in some quarters of the chemical community that Nature avoids N-protonated amides at all costs, especially in nonpolar media.[55] For this reason, an additional line of evidence against rate-determining proton abstraction from $T^{\pm}$ by polyethers, based on the experimental results discussed in sections 3.5-3.7, will be presented here. If proton abstraction by ethers occurs during the rate-determining step of aryl ester aminolysis carried out in chlorobenzene, then the catalytic activities of ether catalysts in this reaction protocol should parallel the proton stabilization energies of the same set of ethers in nonpolar media, such as the gas phase.

Kebarle and coworkers[56] have characterized the proton in terms of its ether affinity in the gas phase. The gas-phase proton is stabilized somewhat less by GLM(3) than by DME(5) (the analog of GLM(3) with the central oxygen replaced by methylene). Apparently the central oxygen in GLM(3) makes it harder for the ether molecule to adopt the conformation(s) necessary to bind to the gas-phase proton. In nonpolar aminolysis the central oxygen in GLM(3) is necessary to achieve reasonable catalysis. DME(5) lies barely above the single-hydrogen-bond baselines. Furthermore, the gas-phase proton seems to prefer to form larger rings with diethers than does the aminolysis catalytic site.

The gas-phase proton is actually stabilized far more by DME(4) and DME(5) than by DME(2), whereas the stabilization of the aminolysis catalytic site by DME(4) and DME(5) is negligible relative to its stabilization by DME(2). In summary, there are significant differences in the behaviors of the gas-phase proton and the rate-determining transition structure involved in ester aminolysis with respect to the stabilization of these species by ethers. These differences suggest that ether catalysts do not abstract protons in the rate-determining step of ester aminolysis carried out in nonpolar media.

Apparently the driving force for linear hydrogen bonding in the gas-phase proton is far stronger than the high entropy price paid for forming larger rings.[56,57] This result is contrary to hydrogen-bonding studies, carried out in solution, involving species more stable than protons (alcohols, amines, etc.).[58] More stable species tend to show little driving force for forming linear hydrogen bonds. For example, α,ω-diol monomethyl ethers (the DME(n) species studied herein with one terminal methyl group in each molecule replaced by hydrogen) form intramolecular hydrogen bonds with the same relative ring-size selectivities[59] shown by the DME(n) series in the aminolysis reaction protocols discussed previously.

The marked difference between naked protons and hydrogens bonded to electronegative atoms can be understood in terms of the internuclear distances between the electronegative atoms surrounding hydrogen in a hydrogen-bonding triad. Naked protons need more stabilization than bound hydrogens, resulting in shorter hydrogen bonds. This translates to shorter heavy-atom internuclear distances resulting in more lone-pair repulsion between electronegative heavy atoms. Lone-pair repulsion between hydrogen-bonded heavy atoms might be expected to give rise to a driving force for linear hydrogen bonds. Linear hydrogen bonds minimize hydrogen-heavy atom distances while maximizing heavy atom-heavy atom distances. Taylor and Kennard have shown[60] that the driving force for linear hydrogen bonding correlates well with

shortness of heavy-atom internuclear distances in solids in a large sample of crystal structures.

The inherent instability of protons probably causes the high affinity for forming linear hydrogen bonds. This affinity makes a proton prefer medium sized α,ω-diethers to DME(2). The kinetically observed species in aminolysis shows the opposite selectivity, leading to the conclusion that the ether catalysts in nonpolar aminolysis protocols are not abstracting protons in the rate-determining step. It has already been demonstrated that the rate-determining step in nonpolar ester aminolysis occurs after binding by ether catalysts to the catalytic site. Therefore it can be concluded that if ethers abstract protons at all in the reactions under study in this work, this activity must occur after the rate-determining step.

If the ammonium proton were abstracted by an amine molecule before aryloxide expulsion, then the reaction kinetics would require a catalytic term which would be second-order in amine and first-order in catalyst (because such an abstraction would have to occur during or before the rate-determining step), which is contrary to what is experimentally observed. If the ether catalyst were to abstract an ammonium proton before aryloxide expulsion then such an abstraction would have to occur before or during the rate-determining step, which has already been ruled out. The only other base in the system capable of abstracting an ammonium proton is the aryloxide nucleofuge; this nucleofuge cannot abstract an ammonium proton before it is expelled. It can therefore be concluded that aryloxide expulsion precedes ammonium proton abstraction.

Aryloxide expulsion from catalyst-complexed $T^{\pm}$ should yield complexed protonated amide, CPA^{+}, which is probably some sort of ion pair, given the nonpolar nature of the reaction medium. At this point CPA^{+} can surrender a proton in one or more steps to the aryloxide nucleofuge. Catalyst or amine may do the actual abstraction, provided that this activity occurs in a fast step. The aryloxide nucleofuge may either

take a proton from some intermediary base in the system to form the final phenol product, or it may abstract a proton directly from CPA^+ (or a less complexed form of CPA^+). This latter possibility minimizes charge separation in nonpolar reaction media, and is therefore more likely; there is currently no direct experimental evidence to support this rationale.

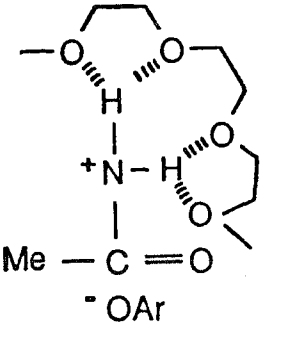

CPA +

Previous work involving transition-structure recognition by polyethers[14,20] (such as the work of Chao and Cram discussed in section 3.11) has involved the use of crown ethers as binding sites which were used to hold a reagent in the proximity of a substrate in order to facilitate a reaction by lowering the entropy hurdle a system has to climb in order to generate a rate-determining transition structure. Primary ammonium ion prosthetic groups attached to reagent species were typically used for this purpose. The objective has been to attempt to mimic the action of enzymes, which employ molecular recognition and transition-structure recognition, in order to bring reagents and substrates together in orientations optimal for chemical reaction.

The new experimental work described in this dissertation has demonstrated transition-structure recognition of a different variety. Polyether binding in this system has done nothing to facilitate substrate-reagent reaction proximity or orientation; conversely, reaction-rate enhancement has been brought about via electrostatic and electronic effects in lieu of orientation effects. This work on glyme-catalyzed ester

aminolysis carried out in aprotic media shows the first demonstrated transition-structure recognition by polyethers in which catalysis involves binding by catalyst at the reaction site rather than at a more remote site. The nature of the transition structure in this system determines both the number of polyether oxygens needed for optimum catalysis, and the optimum spacing between these oxygens.

CONCLUSIONS

Aminolysis of aryl acetates in nonpolar media occurs via a catalyst-complexed tetrahedral intermediate, which breaks down in a subsequent slow step. Catalyst binds either to neutral amine before amine attacks ester, or to the ammonium region of the tetrahedral intermediate formed by attack of amine on ester. Both possibilities yield the same catalyst-complexed tetrahedral intermediate. Polyether catalysts bind up to two oxygens per ammonium proton, in a bifurcated-hydrogen-bonding fashion, to the ammonium proton(s) of the tetrahedral intermediate. Catalytic binding energies can be broken down into bifurcation energies and bridging energies. Catalyst binding weakens a 1,3-dipolar stabilization (of the tetrahedral intermediate) which exists between the positively-charged ammonium nitrogen and the negatively-charged oxyanion of $T^{\pm}$. By binding to the ammonium ion of a tetrahedral intermediate and thereby weakening dipolar stabilization, the catalyst raises the pK_a of the oxyanion, thereby facilitating expulsion of the aryloxide nucleofuge by the oxyanion. Nucleofuge expulsion yields a catalyst-bound N-protonated amide-aryloxide ion pair, such as CPA^+, which shuttles an ammonium proton to aryloxide in one or more steps. It is likely that aryloxide abstracts this proton directly, liberating regenerated catalyst and final reaction products. This chemistry provides the first example of transition-structure recognition by polyether catalysts in which polyethers act by directly modifying the electrostatics and electronics at the reaction site.

The protocol developed and described herein which was used to unravel the mechanistic aspects of glyme-catalyzed aromatic ester aminolysis can probably be used to elucidate reaction mechanisms in other glyme-catalyzed reactions. Glymes are known to catalyze the decomposition of environmentally hazardous chlorinated aromatics like PCB's[61] and dioxins.[62] They also catalyze Ziegler polymerizations,[63] and stabilize cations such as diazonium ions[64] and metal ions.[65] Although catalysis by crown ethers

has been studied extensively,[1-10] there are currently no systematic studies which yield mechanistic descriptions at a molecular level of understanding for glyme-catalyzed reactions, except the work described in this dissertation.

REFERENCES

1. Toner, J. L. in *Crown Ethers and Analogs*; Patai, S., Rappoport, Z., eds.; Wiley: New York, 1989; Chapter 3.
2. Weber, E.; Vögtle, F. *Top. Curr. Chem.* **1981**, *98*, 1-41.
3. (a) Down, J. L.; Lewis, J.; Moore, B.; Wilkinson, G. *J. Chem. Soc.* **1959**, 3767-3773. (b) Pedersen, C. J. *J. Am. Chem. Soc.* **1967**, *89*, 2495-2496. (c) Laidler, D. A.; Stoddart, J. F. in *Crown Ethers and Analogs*; Patai, S., Rappoport, Z., eds.; Wiley: New York, 1989; Chapter 1.
4. Liotta, C. L. in *Synthetic Multidentate Macrocyclic Compounds*; Izatt, R. M.; Christensen, J. J., Eds., Academic Press: New York, 1978; Chapter 3.
5. Liotta, C. L. in *Crown Ethers and Analogs*; Patai, S., Rappoport, Z., eds.; Wiley: New York, 1989; Chapter 2.
6. Weber, E. in *Crown Ethers and Analogs*; Patai, S., Rappoport, Z., eds.; Wiley: New York, 1989; Chapter 5.
7. Liotta, C. L.; Harris, H. P. *J. Am. Chem. Soc.* **1974**, *96*, 2250-2252.
8. Harris, J. M.; Hundley, R. H.; Shannon, T. G.; Struck, E. C. in *Crown Ethers and Phase Transfer Catalysis in Polymer Science*; Mathias, L. J., Carraher, Jr., C. E., Eds.; Plenum: New York, 1984; pp 371-396.
9. Vögtle, F; Weber, E. in *Crown Ethers and Analogs*; Patai, S., Rappoport, Z., Eds., Wiley: New York, 1989; Chapter 4.
10. Bartsch, R. A. in *Crown Ethers and Analogs*; Patai, S., Rappoport, Z., Eds., Wiley: New York, 1989; Chapter 8.
11. Cram, D. J.; Cram, J. M. *Science* **1974**, *183*, 803-809.
12. Cabbiness, D. K.; Magerum, D. W. *J. Am. Chem. Soc.* **1969**, *91*, 6540-6541.
13. Lehn, J.-M. *Struct. Bond.* **1973**, *16*, 1-69.
14. Chao, Y.; Cram, D. J. *J. Am. Chem. Soc.* **1976**, *98*, 1015-1017.

15. Hogan, J. C.; Gandour, R. D. *J. Am. Chem. Soc.* **1980**, *102*, 2865-2866.

16. Vögtle, F.; Sieger, H.; Müller, W. M. *Top. Curr. Chem.* **1981**, *98*, 107-161.

17. Takagi, M.; Veno, K. *Top. Curr. Chem.* **1984**, *121*, 39-65.

18. Shinkai, S.; Manabe, O. *Top. Curr. Chem.* **1984**, *121*, 67-104.

19. Smid, J.; Sinta, R. *Top. Curr. Chem.* **1984**, *121*, 105-156.

20. Shinkai, S.; Koga, K. *J. Inclusion Phenom. Mol. Recognit. Chem.* **1989**, *7*, 267-276; *Chem. Abstr.* **1990**, *112*, 19822a.

21. Hilgenfeld, R.; Saenger, W. *Top. Curr. Chem.* **1982**, *101*, 1-82.

22. Kornel, A.; Rogers, C. *J. Hazard. Mater.* **1985**, *12*, 161-176; *Chem. Abstr.* **1986**, *104*, 135446m.

23. Su, S.-W.; Watson, J. W. *J. Am. Chem. Soc.* **1974**, *96*, 1854-1857.

24. Nagy, O. B.; Reuliaux, V.; Bertrand, N.; Van Der Mensbrugghe, A.; Leseul, J.; Nagy, J. B. *Bull. Soc. Chim. Belg.* **1985**, *94*, 1055-1074.

25. Menger, F. M.; Smith J. H. *J. Am. Chem. Soc.* **1972**, *94*, 3824-3829.

26. Menger, F. M.; Vitale, A. C. *J. Am. Chem. Soc.* **1973**, *95*, 4931-4934.

27. Chan, L. L.; Wong, K. H.; Smid, J. *J. Am. Chem. Soc.* **1970**, *92*, 1955-1963.

28. Yanagida, S.; Takahashi, K.; Okahara, M. *Bull. Chem. Soc. Jpn.* **1978**, *51*, 1294-1299.

29. Hall, R. H.; Stern, E. S. British Patent 695 789, 1953; *Chem. Abstr.* **1954**, *48*, 8816h.

30. Meyer, F.; Krzikalla, H. German Patent 894 110, 1953; *Chem. Abstr.* **1956**, *50*, 4201a.

31. Dermer, O. C.; Hawkins, J. J. *J. Am. Chem. Soc.* **1952**, *74*, 4595-4597.

32. Perry, J. *Introduction to Analytical Gas Chromatography: History, Principles and Practice*; Marcel Dekker: New York, 1981; Chapter 11.

33. Reimschneider, R. U.S. Patent 2 973 388, 1961.

34. Deodhar, V. B.; Dalavoy, V. S.; Nayak, U. R. *Ind. J. Chem.* **1979**, *17B*, 375-378.

35. Dionneau, M. *Bull. Soc. Chim. Fr. Ser. 4* **1910**, *7*, 327-329.

36. Meister, H. *Chem. Ber.* **1963**, *96*, 1688-1696.

37. Braun, J. v.; Danziger, E. *Ber.* **1912**, *45*, 1970-1979.

38. Epsztein, R. *Bull. Soc. Chim. Fr. Ser. 5* **1956**, *23*, 158-160.

39. Detar, D. F. *Computer Programs for Chemistry. I.*; W. A. Benjamin: New York, 1968.

40. Van Etten, R. L. Sebastian, J. F.; Clowes, G. A.; Bender, M. L. *J. Am. Chem. Soc.* **1967**, *89*, 3242-3253.

41. Nishioka, T.; Fugita, T.; Kitamura, K.; Nakajima, M. *J. Org. Chem.* **1975**, *40*, 2520-2525.

42. (a) Lehn, J. M. *Pure Appl. Chem.* **1978**, *50*, 871-892. (b) Izatt, R. M.; Lamb, J. D.; Izatt, N. E.; Rossiter, Jr., B. E.; Christensen, J. J.; Haymore, B. L. *J. Am. Chem. Soc.* **1979**, *101*, 6273-6276. (c) Izatt, R. M.; Izatt, N. E.; Rossiter, B. E.; Christensen, J. J.; Haymore, B. L. *Science* **1978**, *199*, 994-996.

43. Jaffé, H. H. *Chem. Rev.* **1953**, *53*, 191-261.

44. Menger, F. M. *J. Am. Chem. Soc.* **1966**, *88*, 3081-3084.

45. Jencks, W. P. *Acc. Chem. Res.* **1980**, *13*, 161-169.

46. Hammond, G. S. *J. Am. Chem. Soc.* **1955**, *77*, 334-338.

47. (a) Cordes, E. H.; Jencks, W. P. *J. Am. Chem. Soc.* **1962**, *84*, 4319-4328. (b) Jencks, W. P. *Progr. Phys. Org. Chem.* **1964**, *2*, 63-128. (c) Lienhardt, G. E.; Jencks, W. P. *J. Am. Chem. Soc.* **1966**, *88*, 3982-3995. (d) Jencks, W. P. *Chem. Rev.* **1972**, *72*, 705-718.

48. Thornton, E. R. *J. Am. Chem. Soc.* **1967**, *89*, 2915-2927.

49. (a) Porterfield, W. W. *Inorganic Chemistry: A Unified Approach*; Addison-Wesley: London, 1984; Chapter 10. (b) Carey, F. A.; Sundberg, R. J. *Advanced Organic Chemistry Part A: Structure and Mechanisms*, 2nd ed.; Plenum: New York, 1984; Chapter 3.

50. Morton, T. H.; Beauchamp, J. L. *J. Am. Chem. Soc*, **1975**, *97*, 2355-2362.

51. Meotner, M. *J. Am. Chem. Soc.* **1983**, *105*, 4912-4915.

52. The "lock-and-key" model is defined in: Fischer, E. *Ber.* **1894**, *27*, 2985-2993. For discussions of the "induced fit" model, see: (a) Koshland, Jr., D. E. *Proc. Natl. Acad. Sci., U.S.* **1958**, *44*, 98-104. (b) Koshland, Jr., D. E. *J. Biol. Chem.* **1965**, *240*, 1593-1602. (c) Koshland, Jr., D. E. *J. Cell. Comp. Physiol.* **1959**, *54*, Supplement 1, 245-258.

53. Newton, M. D.; Jeffrey, G. A.; Takagi, S. *J. Am. Chem. Soc.* **1979**, *101*, 1997-2002.

54. Perrin, C. L. *Acc. Chem. Res.* **1989**, *22*, 268-275.

55. A referee writes, "It is proposed that the primary product in the ester aminolysis, taking place in a nonpolar solvent, is a phenoxide anion and an N-protonated amide. Only in a fast and kinetically insignificant step is there a proton transfer to create neutral phenol and amide. I must say that I have considerable doubt that ionic products are produced in chlorobenzene especially when one of them is an unstable N-protonated amide. Amides are well known to prefer O-protonation which is resonance stabilized. If the nature of the products is doubtful, then the rationale for the effect of polyethers on the rate, taken literally, is nonsensical ... There is only one way in which the polyether can accelerate the reaction and that is ... accomplished most readily by the polyether acting as a proton shuttling agent.", in response to a paper submitted to *J. Am. Chem. Soc.* covering some of the work described in this dissertation.

56. Sharma, R. B.; Blades, A. T.; Kebarle, P. *J. Am. Chem. Soc.* **1984**, *106*, 510-516.

57. Meotner, M. *J. Am. Chem. Soc.* **1983**, *105*, 4906-4911.

58. Fersht, A. R. *Enzyme Structure and Mechanism*, 2nd Ed.; Freeman: New York, 1985; Chapter 11.

59. Kuhn, L. P.; Wires, R. A. *J. Am. Chem. Soc.* **1964**, *86*, 2161-2165.

60. Taylor, R.; Kennard, O. *Acc. Chem. Res.* **1984**, *17*, 320-326.

61. Brown, Jr., J. F.; Lynch, M. E.; Carnahan, J. C.; Singleton, J. "Abstracts of Papers", 182nd National Meeting of the American Chemical Society, New York, Aug. 1981; ENVR 27.

62. Kornel, A.; Rogers, C. J. *J. Hazard. Mater.* **1985**, *12*, 161-176.

63. See, for example: (a) Suzuki, T.; Chiba, H. Japanese Patent 77 127 994, 1977; *Chem. Abstr.* **1978**, *88*, 191791h. (b) Buben, D.; Bearden, Jr., R.; Wristers, H. J. German Patent 2 318 953, 1973; *Chem. Abstr.* **1974**, *80*, 134068p. (c) Murahashi, S; Nozakura, S.; Hatada, K. *Bull. Chem. Soc. Jpn.* **1961**, *34*, 934-944. (d) Bushick, R. D.; Stearns, R. S.; *J. Polym. Sci., Pt. A-1*, **1966**, *4*(1), 215-232.

64. Bartsch, R. A.; Juri, P. N.; Mills, M. A. *Tetrahedron Lett.* **1979**, 2499-2502.

65. Weber, G.; Saenger, W.; Vögtle, F.; Sieger, H. *Angew. Chem. Int. Ed. Engl.* **1979**, *18*, 226-228.

APPENDIX

Observed Rate Constants for Uncatalyzed, Oligoglyme-catalyzed, and Diether-catalyzed Aminolysis of Substituted Phenyl Acetates at 25° in Chlorobenzene.

Table A1. Observed rate constants for monoglyme-catalyzed butylaminolysis of 4-nitrophenyl acetate at 25° in chlorobenzene.

10^4 [$BuNH_2$], *M*	10^4 [monoglyme], *M*	10^7 k_{obs}, s^{-1}	10^5 $k_{obs}/[BuNH_2]$, M^{-1} s^{-1}
383	60.6	994	260
383	137	1035	271
382	216	1088	285
382	297	1152	302
382	369	1203	315
387	139	1060	274
387	215	1105	286
387	302	1166	301
386	369	1208	313
398	63.9	1028	258
397	220	1137	286
397	293.4	1193	301
397	372.6	1241	313

Table A2. Observed rate constants for diglyme-catalyzed butylaminolysis of 4-nitrophenyl acetate at 25° in chlorobenzene.

10^4 [$BuNH_2$], *M*	10^4 [diglyme], *M*	10^7 k_{obs}, s^{-1}	10^4 k_{obs}/[$BuNH_2$], M^{-1} s^{-1}
389	82.4	1562	40.2
389	167	2141	55.0
388	253.7	2719	70.8
388	337.2	3296	85.0
387	423.9	3879	100
386	84.8	1562	39.4
385	174	2146	54.3
385	252.7	2706	68.5
384	425.6	3862	98.0
387	84.8	1586	40.0
387	171	2175	54.8
386	254.4	2756	69.6
386	340	3328	84.1
385	422.9	3890	98.5

Table A3. Observed rate constants for triglyme-catalyzed butylaminolysis of 4-nitrophenyl acetate at 25° in chlorobenzene.

10^4 [$BuNH_2$], *M*	10^4 [triglyme], *M*	10^7 k_{obs}, s^{-1}	10^5 k_{obs}/[$BuNH_2$], M^{-1} s^{-1}
407	41.5	1606	395
406	88.8	2175	536
406	131	2721	670
406	174	3274	806
405	221	3830	946
401	45.8	1551	387
401	89.9	2116	528
401	135	2670	666
400	178	3229	807
400	224.8	3791	948
403	41.0	1563	388
403	85.4	2137	530
403	131	2672	663
402	174	3211	799
402	222.4	3759	935

Table A4. Observed rate constants for tetraglyme-catalyzed butylaminolysis of 4-nitrophenyl acetate at 25° in chlorobenzene.

10^4 [$BuNH_2$], *M*	10^5 [tetraglyme], *M*	10^7 k_{obs}, s^{-1}	10^4 k_{obs}/[$BuNH_2$], M^{-1} s^{-1}
390	450	1735	44.5
389	999	2492	64.1
389	1455	3224	82.9
388	2539	4888	125
383	491	1692	44.2
382	988	2432	63.7
382	1476	3144	82.3
382	2186	4160	109
381	2454	4564	119
394	481	1772	45.0
394	982	2525	64.1
393	1467	3252	82.8
393	1905	3889	99.0
393	2585	4892	125

Table A5. Observed rate constants for pentaglyme-catalyzed butylaminolysis of 4-nitrophenyl acetate at 25° in chlorobenzene.

10^4 [$BuNH_2$], *M*	10^4 [pentaglyme], *M*	10^7 k_{obs}, s^{-1}	10^4 k_{obs}/[$BuNH_2$], M^{-1} s^{-1}
389	61.0	2031	52.2
389	115	2987	76.8
388	173.5	4024	104
388	233.2	5047	130
387	261.6	5592	145
384	58.1	1984	51.7
384	116	3018	78.6
383	172.5	4039	106
383	228.6	5012	131
382	294.6	6184	162
388	59.5	2019	52.0
387	116	3033	78.4
387	174.7	4071	105
386	230.6	5098	132
386	288.2	6122	159

Table A6. Observed rate constants for hexaglyme-catalyzed butylaminolysis of 4-nitrophenyl acetate at 25° in chlorobenzene.

10^4 [$BuNH_2$], *M*	10^5 [hexaglyme], *M*	10^7 k_{obs}, s^{-1}	10^4 k_{obs}/[$BuNH_2$], M^{-1} s^{-1}
399	498	2030	50.9
388	997	3102	77.9
388	1503	4161	105
397	1995	5253	132
396	2500	6281	159
397	496	2025	51.0
397	986	3106	78.2
396	1515	4152	105
395	2007	5213	132
395	2519	6294	159
400	491	2073	51.8
399	992	3124	78.3
399	1507	4187	105
398	2012	5244	132
397	2478	6273	152

Table A7. Observed rate constants for heptaglyme-catalyzed butylaminolysis of 4-nitrophenyl acetate at 25° in chlorobenzene.

10^4 [$BuNH_2$], *M*	10^5 [heptaglyme], *M*	10^7 k_{obs}, s^{-1}	10^4 k_{obs}/[$BuNH_2$], M^{-1} s^{-1}
377	528	2322	61.6
376	1029	3484	92.7
375	1525	4664	124
375	2044	5882	157
374	2560	7000	187
386	521	2196	56.9
386	1025	2437	89.0
385	1522	4607	120
384	2052	5813	151
384	2536	6990	182
365	517	2056	56.3
364	1021	3243	89.1
364	1520	4358	120
363	2037	5503	152
362	2530	6631	183

Table A8. Observed rate constants for octaglyme-catalyzed butylaminolysis of 4-nitrophenyl acetate at 25° in chlorobenzene.

10^4 [$BuNH_2$], *M*	10^5 [octaglyme], *M*	10^7 k_{obs}, s^{-1}	10^4 k_{obs}/[$BuNH_2$], M^{-1} s^{-1}
390	394	2013	51.6
389	785	3085	79.3
389	1185	4149	107
388	1506	4982	128
387	1979	6260	162
389	392	2037	52.3
389	781	3109	77.6
388	1186	4174	108
388	1579	5222	135
387	1946	6208	160
407	400	2189	53.7
406	800	3326	81.9
405	1589	5551	137
405	1977	6629	164

Table A9. Observed rate constants for uncatalyzed butylaminolysis of 3-chlorophenyl acetate at 25° in chlorobenzene.

10^3 [$BuNH_2$], *M*	$10^7 k_{obs}$, s^{-1}	$10^6 k_{obs}/[BuNH_2]$, $M^{-1} s^{-1}$
396	1589	401
396	1578	398
396	1504	380
396	1495	378
396	1458	368
474	2253	475
474	2220	468
474	2184	461
474	2141	452
474	2142	452
595	3565	599
595	3504	589
595	3495	587
595	3456	581
595	3374	567
673	4717	701
673	4668	694
673	4641	690
673	4555	677
673	4571	679

Table A10. Observed rate constants for uncatalyzed butylaminolysis of 3-bromophenyl acetate at 25° in chlorobenzene.

10^4 [$BuNH_2$], *M*	10^7 k_{obs}, s^{-1}	10^7 k_{obs}/[$BuNH_2$], M^{-1} s^{-1}
1968	425.1	2160
1968	419.3	2131
1968	416.8	2118
1968	414.8	2108
2420	638.0	2636
2420	631.7	2610
2420	629.7	2602
2420	600.7	2482
2420	596.3	2464
2902	993.5	3424
2902	969.6	3341
2902	898.4	3096
2902	910.3	3137
2902	918.7	3166
3429	1262	3680
3429	1276	3721
3429	1310	3820
3429	1293	3771
3429	1297	3782
3765	1545	4104
3765	1516	4027
3765	1512	4016
3765	1531	4066
3765	1486	3947
5038	2930	5816
5038	2844	5645
5038	2810	5578
5038	2870	5697
5038	2875	5707

Table A11. Observed rate constants for uncatalyzed butylaminolysis of 3-cyanophenyl acetate at 25° in chlorobenzene.

10^4 [$BuNH_2$], *M*	$10^7 k_{obs}$, s^{-1}	$10^6 k_{obs}/[BuNH_2]$, $M^{-1} s^{-1}$
956.6	412.8	431.5
956.6	411.5	430.2
956.6	431.7	451.3
956.6	434.4	454.1
956.6	405.6	424.0
1534	1029	670.8
1534	1043	679.9
1534	1024	667.5
1534	1038	676.7
2547	2985	1172
2547	2982	1171
2547	2975	1168
2547	2969	1166
3060	4290	1402
3060	4323	1413
3060	4286	1401
3060	4285	1400
3060	4335	1417

Table A12. Observed rate constants for uncatalyzed butylaminolysis of 4-cyanophenyl acetate at 25° in chlorobenzene.

10^3 [$BuNH_2$], *M*	10^7 k_{obs}, s^{-1}	10^5 k_{obs}/[$BuNH_2$], M^{-1} s^{-1}
71.7	1114	155
71.7	1116	156
71.7	1122	156
71.7	1114	155
71.7	1098	153
90.9	1819	200
90.9	1811	199
90.9	1830	201
90.9	1812	199
90.9	1837	202
111	2755	248
111	2855	257
111	2753	248
111	2846	256
111	2839	256
149	5258	353
149	5237	351
149	5216	350
149	5216	350
149	5255	353

Table A13. Observed rate constants for monoglyme-catalyzed butylaminolysis of 3-chlorophenyl acetate at 25° in chlorobenzene.

10^4 [$BuNH_2$], *M*	10^4 [monoglyme], *M*	10^8 k_{obs}, s^{-1}	10^7 k_{obs}/[$BuNH_2$], M^{-1} s^{-1}
1530	195	2755	1801
1526	401.4	2763	1811
1516	1013	3078	2030
1497	198	2410	1610
1494	404.7	2761	1848
1491	606.1	2792	1873
1488	805.6	2830	1902
1484	1007	2967	1999
1500	194	2475	1650
1497	404.7	2697	1802
1494	610.8	2645	1770
1491	794.3	2709	1817
1488	1011	2751	1850

Table A14. Observed rate constants for monoglyme-catalyzed butylaminolysis of 3-bromophenyl acetate at 25° in chlorobenzene.

10^4 [$BuNH_2$], *M*	10^4 [monoglyme], *M*	10^8 k_{obs}, s^{-1}	10^7 $k_{obs}/[BuNH_2]$, M^{-1} s^{-1}
1504	158	2987	1986
1497	601.4	3156	2108
1494	794.3	3228	2161
1491	1005	3344	2243
1537	193	2949	1919
1534	404.3	3047	1986
1530	608.3	3123	2041
1527	810.6	3197	2094
1524	1023	3202	2167
1563	403	3190	2041
1559	605.7	3297	2115
1556	801.9	3358	2158
1553	997.3	3411	2196

Table A15. Observed rate constants for monoglyme-catalyzed butylaminolysis of 3-cyanophenyl acetate at 25° in chlorobenzene.

10^4 [$BuNH_2$], *M*	10^4 [monoglyme], *M*	10^7 k_{obs}, s^{-1}	10^7 k_{obs}/[$BuNH_2$], M^{-1} s^{-1}
1524	188	991.0	6503
1521	392.0	1027	6752
1518	595.9	1055	6950
1514	801.6	1100	7266
1511	1008	1134	7505
1485	191	964.6	6496
1482	394.1	978.9	6660
1478	598.8	1042	7050
1475	803.4	1068	7241
1472	1002	1095	7439
1493	192	961.3	6439
1490	400.0	994.0	6671
1481	1007	1099	7241

Table A16. Observed rate constants for monoglyme-catalyzed butylaminolysis of 4-cyanophenyl acetate at 25° in chlorobenzene.

10^5 [$BuNH_2$], *M*	10^4 [monoglyme], *M*	10^8 k_{obs}, s^{-1}	10^6 k_{obs}/[$BuNH_2$], M^{-1} s^{-1}
5913	91.4	5723	967.9
5894	398.8	6476	1099
5888	504.0	6598	1121
6064	95.4	5962	983.1
6058	193	6170	1018
6051	297	6431	1063
6045	402.1	6686	1106
5596	92.7	5401	965.2
5590	190	5623	1006
5584	295	5782	1035
5578	402.9	6053	1085
5572	500.2	6248	1121

Table A17. Observed rate constants for diglyme-catalyzed butylaminolysis of 3-chlorophenyl acetate at 25° in chlorobenzene.

10^4 [$BuNH_2$], *M*	10^4 [diglyme], *M*	10^8 k_{obs}, s^{-1}	10^7 k_{obs}/[$BuNH_2$], M^{-1} s^{-1}
1526	100	2759	1808
1524	202	3086	2025
1522	303	3274	2151
1520	402	3635	2931
1518	507.2	3842	2531
1511	207	2958	1958
1509	305.1	3300	2187
1507	400.8	3697	2453
1505	499.9	3919	2604
1547	203	3031	1959
1545	307.7	3377	2186
1543	402.3	3648	2364
1541	506.8	4106	2665

Table A18. Observed rate constants for diglyme-catalyzed butylaminolysis of 3-bromophenyl acetate at 25° in chlorobenzene.

10^4 [$BuNH_2$], *M*	10^4 [diglyme], *M*	10^8 k_{obs}, s^{-1}	10^7 k_{obs}/[$BuNH_2$], M^{-1} s^{-1}
1540	102	2964	1925
1535	302.9	3574	2328
1533	397.2	3829	2498
1531	500.4	4287	2800
1539	103	2825	1836
1537	203	3104	2020
1535	304.3	3405	2218
1533	408.1	3669	2393
1531	504.3	4081	2666
1523	201	3123	2051
1521	300.2	3405	2239
1519	398.1	3669	2415
1517	500.2	4081	2690

Table A19. Observed rate constants for diglyme-catalyzed butylaminolysis of 3-cyanophenyl acetate at 25° in chlorobenzene.

10^4 [$BuNH_2$], *M*	10^4 [diglyme], *M*	10^7 k_{obs}, s^{-1}	10^6 $k_{obs}/[BuNH_2]$, M^{-1} s^{-1}
1509	98.8	1089	721.7
1507	204	1254	832.1
1505	305.8	1412	938.2
1503	400.6	1570	1045
1501	486.5	1748	1165
1512	104	1093	722.9
1510	205	1242	822.5
1508	303.6	1407	933.0
1506	402.0	1571	1043
1504	505.8	1745	1160
1518	100	1059	697.6
1516	205	1222	806.1
1513	307.0	1393	920.7
1511	401.1	1561	1033
1509	499.0	1726	1144

Table A20. Observed rate constants for diglyme-catalyzed butylaminolysis of 4-cyanophenyl acetate at 25° in chlorobenzene.

10^5 [$BuNH_2$], *M*	10^4 [diglyme], *M*	10^7 k_{obs}, s^{-1}	10^6 k_{obs}/[$BuNH_2$], M^{-1} s^{-1}
5905	49.9	681.2	1154
5900	101	822.3	1394
5896	151	961.1	1630
5892	204	1095	1858
6088	52.6	708.6	1164
6084	103	853.6	1403
6080	152	996.8	1639
6075	202	1147	1888
6071	253	1278	2105
6056	51.6	703.0	1161
6051	104	857.9	1418
6047	151	989.6	1637
6039	249	1273	2108

Table A21. Observed rate constants for triglyme-catalyzed butylaminolysis of 3-chlorophenyl acetate at 25° in chlorobenzene.

10^4 [$BuNH_2$], *M*	10^4 [triglyme], *M*	10^8 k_{obs}, s^{-1}	10^7 k_{obs}/[$BuNH_2$], M^{-1} s^{-1}
1503	100	2893	1925
1500	213.0	3149	2099
1498	302.9	3350	2236
1493	494.6	3934	2635
1504	99.1	2771	1842
1501	203.8	3041	2022
1499	299.6	3380	2255
1496	407.5	3582	2394
1494	503.0	3946	2641
1494	111	2993	2003
1492	203.8	3127	2096
1489	298.0	3424	2300
1487	391.4	3631	2442
1484	490.4	3954	2664

Table A22. Observed rate constants for triglyme-catalyzed butylaminolysis of 3-bromophenyl acetate at 25° in chlorobenzene.

10^4 [$BuNH_2$], *M*	10^4 [triglyme], *M*	10^8 k_{obs}, s^{-1}	10^7 k_{obs}/[$BuNH_2$], M^{-1} s^{-1}
1506	100	2790	1853
1503	198.5	3180	2116
1500	301.1	3550	2367
1498	397.1	3758	2509
1495	499.2	4101	2816
1507	95.2	2790	1851
1504	200.2	3185	2118
1502	295.8	3502	2332
1499	394.5	3882	2590
1497	493.1	4155	2776
1485	195.6	2332	2244
1482	304.0	3617	2441
1480	394.3	3955	2672
1477	490.7	4231	2865

Table A23. Observed rate constants for triglyme-catalyzed butylaminolysis of 3-cyanophenyl acetate at 25° in chlorobenzene.

10^4 [$BuNH_2$], *M*	10^4 [triglyme], *M*	10^7 k_{obs}, s^{-1}	10^6 $k_{obs}/[BuNH_2]$, M^{-1} s^{-1}
1483	100	1176	793.0
1480	202.9	1445	976.4
1477	298.5	1679	1137
1475	395.1	1923	1304
1472	498.6	2153	1463
1509	200.0	1483	982.8
1506	299.1	1708	1134
1504	397.3	1921	1272
1501	495.3	2147	1430
1495	100	1206	806.7
1492	200.2	1423	953.8
1490	300.2	1657	1112
1487	393.1	1856	1248
1485	494.0	2102	1415

Table A24. Observed rate constants for triglyme-catalyzed butylaminolysis of 4-cyanophenyl acetate at 25° in chlorobenzene.

10^5 [$BuNH_2$], *M*	10^4 [triglyme], *M*	10^7 k_{obs}, s^{-1}	10^6 k_{obs}/[$BuNH_2$], M^{-1} s^{-1}
6276	50.3	902.7	1438
6270	101	1152	1837
6265	151	1415	2259
6259	200.7	1662	2655
6254	247.5	1881	3008
6038	51.2	842.5	1395
6033	101	1090	1807
6028	150	1340	2223
6022	201.0	1585	2632
6017	251.2	1807	3003
5839	50.1	791.0	1355
5828	149	1266	2172
5823	190.4	1492	2562

Table A25. Observed rate constants for tetraglyme-catalyzed butylaminolysis of 3-chlorophenyl acetate at 25° in chlorobenzene.

10^4 [$BuNH_2$], *M*	10^5 [tetraglyme], *M*	10^8 k_{obs}, s^{-1}	10^7 k_{obs}/[$BuNH_2$], M^{-1} s^{-1}
1475	2978	3673	2490
1472	3620	3939	2676
1469	4767	4299	2927
1509	972	3074	2037
1502	2928	3771	2511
1499	4012	4173	2784
1496	4614	4410	2948
1461	991	2995	2050
1457	1903	3405	2337
1454	2875	3730	2565
1451	3820	4034	2780
1448	4753	4311	2977

Table A26. Observed rate constants for tetraglyme-catalyzed butylaminolysis of 3-bromophenyl acetate at 25° in chlorobenzene.

10^4 [$BuNH_2$], *M*	10^5 [tetraglyme], *M*	10^8 k_{obs}, s^{-1}	10^7 k_{obs}/[$BuNH_2$], M^{-1} s^{-1}
1545	998	3487	2257
1541	2219	3874	2514
1538	3228	4392	2856
1535	4066	4634	3025
1531	5066	5160	3362
1545	997	3725	2120
1541	2151	3982	2584
1538	2925	4356	2832
1535	3430	4562	2985
1531	4723	5074	3314
1525	976	3462	2270
1522	2054	3878	2548
1519	3061	4224	2781
1515	3914	4631	3057
1512	4817	5285	3495

Table A27. Observed rate constants for tetraglyme-catalyzed butylaminolysis of 3-cyanophenyl acetate at 25° in chlorobenzene.

10^4 [$BuNH_2$], *M*	10^5 [tetraglyme], *M*	10^7 k_{obs}, s^{-1}	10^6 k_{obs}/[$BuNH_2$], M^{-1} s^{-1}
1465	1105	1143	780.2
1462	2295	1484	1015
1459	3121	1726	1183
1456	4116	2078	1427
1453	5013	2337	1608
1485	964	1133	763.0
1482	2254	1508	1018
1479	3065	1777	1212
1476	4052	2056	1393
1473	4843	2308	1567
1468	966	1088	741.1
1464	2123	1456	994.5
1461	3124	1739	1190
1458	4018	2045	1403
1455	4029	2083	1432

Table A28. Observed rate constants for the tetraglyme-catalyzed butylaminolysis of 4-cyanophenyl acetate at 25°C in chlorobenzene.

10^5 [$BuNH_2$], *M*	10^5 [tetraglyme], *M*	10^7 k_{obs}, s^{-1}	10^6 k_{obs}/[$BuNH_2$], M^{-1} s^{-1}
5665	470	837.77	1479
5659	955	1111	1963
5653	1482	1383	2247
5647	2275	1776	3145
5640	2754	2011	3566
5778	485	839.9	1454
5772	1004	1135	1966
5766	1475	1417	2458
5760	2206	1715	3116
5753	2672	2047	3558
5908	476	861.1	1458
5901	963	1131	1917
5895	1478	1409	2390
5889	2265	1835	3116
5882	2698	2054	3492

Table A29. Observed rate constants for the octaglyme-catalyzed butylaminolysis of 3-chlorophenyl acetate at 25°C in chlorobenzene.

10^4 [$BuNH_2$], *M*	10^5 [octaglyme], *M*	10^8 k_{obs}, s^{-1}	10^7 k_{obs}/[$BuNH_2$], M^{-1} s^{-1}
1527	1171	3716	2434
1521	1967	4544	2988
1515	3044	5198	3431
1510	3847	5543	3671
1504	4768	6068	4035
1459	1032	3439	2357
1454	1974	4160	2861
1449	2850	4736	3269
1443	3671	5161	3577
1438	5134	5867	4080
1523	953	4242	2785
1517	1894	4580	3019
1512	2971	5418	2583
1506	3910	5955	3954
1500	4872	6355	4237

Table A30. Observed rate constants for octaglyme-catalyzed butylaminolysis of 3-bromophenyl acetate at 25° in chlorobenzene.

10^4 [$BuNH_2$], *M*	10^5 [octaglyme], *M*	10^8 k_{obs}, s^{-1}	10^7 $k_{obs}/[BuNH_2]$, M^{-1} s^{-1}
1523	996	4126	2709
1517	1781	4835	3187
1512	2840	5759	3809
1506	3558	6179	4103
1500	4375	6761	4507
1528	1042	4447	2910
1522	1967	5322	3497
1516	2768	5990	3951
1511	3708	6655	4404
1492	1411	4297	2880
1486	2680	5424	3651
1481	3731	6011	4059
1475	4568	6433	4361

Table A31. Observed rate constants for octaglyme-catalyzed butylaminolysis of 3-cyanophenyl acetate at 25° in chlorobenzene.

10^4 [$BuNH_2$], *M*	10^5 [octaglyme], *M*	10^7 k_{obs}, s^{-1}	10^6 k_{obs}/[$BuNH_2$], M^{-1} s^{-1}
1467	1146	1281	873.2
1462	2098	1871	1280
1457	3000	2340	1606
1451	3876	2833	1952
1446	4847	3276	2266
1471	1190	1360	924.5
1466	2091	1888	1288
1460	3008	2403	1646
1455	3930	2886	1984
1449	4879	3392	2341
1456	2034	1787	1227
1452	2998	2291	1578
1447	3934	2801	1936
1442	4866	3315	2299

Table A32. Observed rate constants for octaglyme-catalyzed butylaminolysis of 4-cyanophenyl acetate at 25° in chlorobenzene.

10^5 [$BuNH_2$], *M*	10^5 [octaglyme], *M*	10^7 k_{obs}, s^{-1}	10^6 k_{obs}/[$BuNH_2$], M^{-1} s^{-1}
6254	509	1272	2034
6242	898	1682	2695
6231	1379	2141	3436
6219	1865	2524	4059
6207	2246	2890	4656
5806	504	1134	1952
5795	1090	1686	2909
5784	1475	2016	3486
5774	2011	2436	4219
5763	2471	2865	4971
5569	512	1064	1910
5558	955	1484	2670
5548	1437	1878	3385
5538	1970	2307	4166

Table A33. Observed rate constants for 1,3-dimethoxypropane-catalyzed butylaminolysis of 4-nitrophenyl acetate at 25° in chlorobenzene.

10^5 [$BuNH_2$], *M*	10^4 [dimethoxypropane], *M*	10^7 k_{obs}, s^{-1}	10^6 k_{obs}/[$BuNH_2$], M^{-1} s^{-1}
3984	94.8	1004	2520
3979	196	1023	2568
3974	296	1044	2620
3969	401.0	1079	2719
3964	497.7	1098	2770
3973	96.7	996.7	2509
3968	202	1015	2558
3963	290	1034	2609
3958	396.3	1062	2683
3954	495.8	1086	2747
3858	94.8	959.7	2488
3853	198	981.4	2547
3849	296	996.5	2589
3844	399.4	1025	2666
3839	491.4	1048	2730

Table A34. Observed rate constants for 1,4-dimethoxybutane-catalyzed butylaminolysis of 4-nitrophenyl acetate at 25° in chlorobenzene.

10^5 [$BuNH_2$], *M*	10^4 [dimethoxybutane], *M*	10^7 k_{obs}, s^{-1}	10^6 k_{obs}/[$BuNH_2$], M^{-1} s^{-1}
3986	97.4	1058	2654
3981	196	1084	2723
3975	290.1	1095	2755
3970	392.6	1130	2846
3964	489.8	1153	2909
3969	98.0	1040	2620
3964	195	1064	2684
3958	294.3	1086	2744
3953	394.8	1109	2805
3947	487.6	1129	2860
3966	97.2	1025	2584
3961	109.4	1035	2613

Table A35. Observed rate constants for 1,5-dimethoxypentane-catalyzed butylaminolysis of 4-nitrophenyl acetate at 25° in chlorobenzene.

10^5 [$BuNH_2$], *M*	10^4 [dimethoxypropane], *M*	10^7 k_{obs}, s^{-1}	10^6 k_{obs}/[$BuNH_2$], M^{-1} s^{-1}
4191	101	1147	2737
4184	197	1175	2808
4178	296.2	1204	2882
4172	395.0	1229	2946
4165	493.9	1240	2977
4003	98.8	1122	2803
3997	192	1159	2900
3991	299.9	1176	2947
3984	397.0	1207	3030
3978	493.4	1223	3074
4066	99.3	1105	2718
4060	196	1132	2788
4053	295.2	1156	2852
4047	392.6	1182	2921
4041	488.2	1208	2989

Table A36. Observed rate constants for 1,6-dimethoxyhexane-catalyzed butylaminolysis of 4-nitrophenyl acetate at 25° in chlorobenzene.

10^5 [$BuNH_2$], *M*	10^4 [dimethoxyhexane], *M*	$10^7 k_{obs}$, s^{-1}	$10^6 k_{obs}/[BuNH_2]$, $M^{-1} s^{-1}$
3811	110	969.5	2544
3835	218	988.4	2584
3828	322.5	1004	2623
3822	426.9	1028	2697
3815	528.3	1043	2734
3851	96.9	972.4	2525
3838	292.1	1003	2613
3832	392.8	1014	2646
3825	496.2	1045	2732
3804	96.1	959.0	2521
3797	194	973.4	2564
3791	295.7	994.9	2624
3785	388.5	1012	2673
3778	492.6	1037	2745

Table A37. Observed rate constants for 1,7-dimethoxyheptane-catalyzed butylaminolysis of 4-nitrophenyl acetate at 25° in chlorobenzene.

10^5 [$BuNH_2$], *M*	10^4 [dimethoxyheptane], *M*	10^7 k_{obs}, s^{-1}	10^6 k_{obs}/[$BuNH_2$], M^{-1} s^{-1}
3823	99.3	982.9	2571
3816	199	993.8	2604
3806	299.3	1011	2656
3801	393.0	1033	2718
3794	489.5	1051	2770
3911	97.7	998.5	2553
3904	194	1017	2605
3896	295.0	1037	2662
3889	392.8	1067	2744
3882	489.1	1086	2798
3941	96.7	1023	2596
3933	197	1045	2657
3926	295.0	1061	2702
3919	390.4	1081	2758
3911	490.3	1103	2820

Table A38. Observed rate constants for 1,8-dimethoxyoctane-catalyzed butylaminolysis of 4-nitrophenyl acetate at 25° in chlorobenzene.

10^5 [$BuNH_2$], *M*	10^5 [dimethoxyoctane], *M*	10^7 k_{obs}, s^{-1}	10^6 $k_{obs}/[BuNH_2]$, M^{-1} s^{-1}
3823	99.3	982.9	2571
3816	199	993.8	2604
3806	299.3	1011	2656
3801	393.0	1033	2718
3794	489.5	1051	2770
3911	97.7	998.5	2553
3904	194	1017	2605
3896	295.0	1037	2662
3889	392.8	1067	2744
3882	489.1	1086	2798
3941	96.7	1023	2596
3933	197	1045	2657
3926	295.0	1061	2702
3919	390.4	1081	2758
3911	490.3	1103	2820

Table A39. Observed rate constants for 1,9-dimethoxynonane-catalyzed butylaminolysis of 4-nitrophenyl acetate at 25° in chlorobenzene.

10^5 [$BuNH_2$], *M*	10^5 [dimethoxynonane], *M*	10^7 k_{obs}, s^{-1}	10^6 k_{obs}/[$BuNH_2$], M^{-1} s^{-1}
3943	1989	1040	2638
3935	2941	1059	2691
3926	3927	1086	2766
3918	4914	1112	2838
3881	985	995.2	2564
3872	1988	1019	2632
3864	2941	1038	2686
3855	3937	1068	2770
3847	4890	1089	2831
3917	985	1000	2553
3909	2000	1021	2612
3883	4881	1091	2810

Table A40. Observed rate constants for 1,10-dimethoxydecane-catalyzed butylaminolysis of 4-nitrophenyl acetate at 25° in chlorobenzene.

10^5 [$BuNH_2$], *M*	10^5 [dimethoxydecane], *M*	10^7 k_{obs}, s^{-1}	10^6 k_{obs}/[$BuNH_2$], M^{-1} s^{-1}
3709	989	916.7	2472
3700	1942	951.3	2571
3691	2917	989.5	2681
3683	3877	1024	2780
3674	4890	1065	2899
3832	983	960.2	2506
3823	1994	997.8	2610
3814	2972	1031	2703
3805	3927	1067	2804
3796	4903	1101	2900
3862	976	969.6	2511
3853	1982	1001	2598
3844	2929	1040	2706
3835	3978	1082	2821
3826	4866	1114	2912

Table A41. Observed rate constants for 1,12-dimethoxydodecane-catalyzed butylaminolysis of 4-nitrophenyl acetate at 25° in chlorobenzene.

10^5 [$BuNH_2$], *M*	10^4 [dimethoxydodecane], *M*	10^7 k_{obs}, s^{-1}	10^6 k_{obs}/[$BuNH_2$], M^{-1} s^{-1}
4042	103	1091	2699
4030	210.2	1111	2757
4019	318.5	1136	2827
4008	413.7	1142	2849
3996	520.7	1164	2913
4043	97.6	1091	2698
4032	195.9	1108	2748
4021	292.3	1127	2803
4011	391.9	1148	2862
4001	492.4	1162	2904
4037	97.7	1090	2700
4027	197.6	1111	2759
4016	291.8	1124	2799
4009	387.8	1145	2858
3995	487.6	1165	2916

Table A42. Observed rate constants for 1,2-dimethoxyethane-catalyzed methylbutylaminolysis of 4-nitrophenyl acetate at 25° in chlorobenzene.

10^5 [MeBuNH], *M*	10^4 [dimethoxyethane], *M*	$10^7 k_{obs}$, s^{-1}	$10^6 k_{obs}$/[MeBuNH], $M^{-1} s^{-1}$
4131	94.9	2434	5892
4127	200	2475	5997
4123	281	2507	6081
4119	388.4	2554	6201
4114	491.9	2591	6298
3961	94.9	2308	5827
3957	192	2355	5951
3953	300	2391	6049
3949	393.1	2429	6151
3945	497.0	2472	6266
3900	86.9	2265	5808
3896	194	2312	5934
3892	291	2355	6051
3888	392.0	2399	6170
3884	499.2	2451	6311

Table A43. Observed rate constants for 1,3-dimethoxypropane-catalyzed methylbutylaminolysis of 4-nitrophenyl acetate at 25° in chlorobenzene.

10^5 [MeBuNH], *M*	10^4 [dimethoxypropane], *M*	$10^7 k_{obs}$, s^{-1}	$10^6 k_{obs}$/[MeBuNH], $M^{-1} s^{-1}$
3969	91.3	2262	5699
3964	201	2286	5767
3959	297	2315	5847
3955	396.0	2315	5853
3950	494.5	2344	5934
3927	96.7	2241	5707
3922	195	2258	5757
3918	291	2277	5811
3913	286.6	2296	5868
3908	496.1	2320	5937
3998	98.2	2301	5755
3993	197	2317	5803
3989	296	2344	5876
3984	395.4	2345	5911

Table A44. Observed rate constants for 1,4-dimethoxybutane-catalyzed methylbutylaminolysis of 4-nitrophenyl acetate at 25° in chlorobenzene.

10^5 [MeBuNH], *M*	10^4 [dimethoxybutane], *M*	$10^7 k_{obs}$, s^{-1}	$10^6 k_{obs}$/[MeBuNH], $M^{-1} s^{-1}$
4069	98.3	2310	5677
4064	201	2329	5731
4058	295.4	2345	5779
4052	395.6	2365	5837
4047	491.4	2382	5886
4078	99.1	2303	5647
4073	195	2323	5703
4067	294.8	2344	5763
4061	396.5	2358	5806
4056	495.6	2378	5863
4166	100	2358	5660
4160	197	2381	5724
4154	294.0	2400	5778
4149	393.1	2423	5840
4143	493.1	2445	5902

Table A45. Observed rate constants for 1,5-dimethoxypentane-catalyzed methylbutylaminolysis of 4-nitrophenyl acetate at 25° in chlorobenzene.

10^5 [MeBuNH], *M*	10^4 [dimethoxypentane], *M*	10^7 k_{obs}, s^{-1}	10^6 k_{obs}/[MeBuNH], M^{-1} s^{-1}
3882	97.0	2151	5541
3876	198	2171	5601
3870	297.2	2185	5646
3864	394.5	2203	5701
3858	490.2	2218	5749
3862	98.5	2129	5513
3856	192	2147	5568
3850	292.7	2157	5603
3844	392.1	2174	5656
3839	491.4	2188	5699
3865	99.3	2145	5550
3859	195	2164	5608
3833	292.2	2174	5642
3847	389.4	2192	5698
3841	490.1	2109	5751

Table A46. Observed rate constants for 1,6-dimethoxyhexane-catalyzed methylbutylaminolysis of 4-nitrophenyl acetate at 25° in chlorobenzene.

10^5 [MeBuNH], *M*	10^4 [dimethoxyhexane], *M*	$10^7 k_{obs}$, s^{-1}	$10^6 k_{obs}$/[MeBuNH], $M^{-1} s^{-1}$
3923	97.4	2195	5595
3917	198	2208	5637
3910	295.0	2226	5693
3903	393.4	2239	5737
3897	492.6	2252	5779
3891	98.1	2186	5618
3885	199	2196	5653
3878	295.0	2211	5701
3872	397.4	2226	5749
3865	493.7	2240	5796
3927	97.4	2193	5584
3920	198	2210	5638
3914	295.2	2222	5677
3907	391.8	2233	5715
3900	494.4	2255	5782

Table A47. Observed rate constants for 1,7-dimethoxyheptane-catalyzed methylbutylaminolysis of 4-nitrophenyl acetate at 25° in chlorobenzene.

10^5 [MeBuNH], *M*	10^4 [dimethoxyheptane], *M*	$10^7 k_{obs}$, s^{-1}	$10^6 k_{obs}$/[MeBuNH], $M^{-1} s^{-1}$
3897	99.1	2201	5648
3890	196	2212	5686
3883	294.4	2228	5738
3876	393.7	2245	5792
3869	492.3	2256	5831
4050	80.9	2285	5642
4043	198	2299	5686
4035	294.4	2314	5735
4028	342.4	2328	5780
4020	495.2	2341	5823
3979	100.1	2249	5652
3972	196	2260	5690
3965	294.4	2277	5743
3957	393.0	2288	5782
3950	495.4	2304	5833

Table A48. Observed rate constants for 1,8-dimethoxyoctane-catalyzed methylbutylaminolysis of 4-nitrophenyl acetate at 25° in chlorobenzene.

10^5 [MeBuNH], *M*	10^4 [dimethoxyoctane], *M*	$10^7 k_{obs}$, s^{-1}	$10^6 k_{obs}$/[MeBuNH], $M^{-1} s^{-1}$
3905	113	2189	5605
3896	222.0	2202	5652
3887	332.6	2216	5701
3870	555.9	2245	5801
3940	116	2220	5635
3941	224.5	2236	5688
3922	333.6	2251	5739
3913	443.1	2267	5794
3904	552.2	2278	5835
3882	111	2191	5644
3873	220.7	2208	5701
3864	335.6	2224	5756
3856	445.0	2236	5790
3847	555.4	2248	5844

Table A49. Observed rate constants for 1,9-dimethoxynonane-catalyzed methylbutylaminolysis of 4-nitrophenyl acetate at 25° in chlorobenzene.

10^5 [MeBuNH], *M*	10^5 [dimethoxynonane], *M*	$10^7 k_{obs}$, s^{-1}	$10^6 k_{obs}$/[MeBuNH], $M^{-1} s^{-1}$
3799	979	2133	5614
3722	1818	2141	5646
3783	2936	2156	5699
3774	3927	2165	5737
3766	4941	2174	5773
3933	997	2211	5622
3926	1828	2217	5647
3916	2976	2234	5705
3908	3932	2244	5742
3899	4943	2258	5791
3934	2919	2247	5712
3917	4890	2266	5785

Table A50. Observed rate constants for 1,10-dimethoxydecane-catalyzed methylbutylaminolysis of 4-nitrophenyl acetate at 25° in chlorobenzene.

10^5 [MeBuNH], *M*	10^4 [dimethoxydecane], *M*	$10^7 k_{obs}$, s^{-1}	$10^6 k_{obs}$/[MeBuNH], $M^{-1} s^{-1}$
3926	102	2181	5555
3917	202.7	2192	5596
3908	304.6	2209	5653
3898	403.2	2215	5682
3889	504.4	2228	5729
3902	100	2178	5582
3893	203.0	2186	5615
3883	305.8	2200	5666
3874	405.6	2213	5712
3865	510.0	2226	5759
3883	102	2163	5570
3874	205.3	2174	5612
3864	303.6	2184	5652
3855	405.1	2200	5707
3846	508.2	2213	5754

Table A51. Observed rate constants for 1,12-dimethoxydodecane-catalyzed methylbutylaminolysis of 4-nitrophenyl acetate at 25° in chlorobenzene.

10^5 [MeBuNH], *M*	10^5 [dimethoxydodecane], *M*	$10^7 k_{obs}$, s^{-1}	$10^6 k_{obs}$/[MeBuNH], $M^{-1} s^{-1}$
3889	976	2162	5559
3879	1952	2175	5607
3869	2869	2180	5635
3859	3874	2193	5683
3849	4818	2197	5708
3863	976	2144	5550
3853	1942	2154	5590
3843	2882	2161	5623
3833	3833	2168	5656
3975	976	2213	5567
3955	2896	2237	5656
3944	3872	2240	5680
3934	4817	2249	5717

Table A52. Observed rate constants for diglyme-catalyzed methylbutylaminolysis of 4-nitrophenyl acetate at 25° in chlorobenzene.

10^5 [MeBuNH], *M*	10^4 [diglyme], *M*	$10^7 k_{obs}$, s^{-1}	$10^6 k_{obs}$/[MeBuNH], $M^{-1} s^{-1}$
3971	102	2289	5764
3966	197	2343	5908
3960	295.3	2402	6066
3955	391.8	2465	6234
3949	488.3	2517	6374
4025	103	2312	5744
4019	193	2369	5895
4013	296.8	2424	6040
4008	393.3	2496	6228
4002	491.7	2544	6357
3979	100	2295	5768
3974	201	2357	5931
3968	294.3	2419	6096
3963	396.2	2478	6253
3957	492.6	2535	6406

Table A53. Observed rate constants for triglyme-catalyzed methylbutylaminolysis of 4-nitrophenyl acetate at 25° in chlorobenzene.

10^5 [MeBuNH], *M*	10^4 [triglyme], *M*	$10^7 k_{obs}$, s^{-1}	$10^6 k_{obs}$/[MeBuNH], $M^{-1} s^{-1}$
3993	96.7	2328	5830
3986	198.1	2414	6056
3979	284.0	2493	6265
3972	396.7	2576	6485
3965	482.3	2653	6691
4043	100	2359	5835
4036	192.3	2444	6056
4029	291.7	2517	6247
4022	387.2	2592	6445
4015	485.8	2683	6682
4256	99.1	2528	5940
4248	196.9	2620	6168
4241	295.6	2708	6385
4234	386.5	2794	6599
4226	490.0	2880	6815

VITA

John C. Hogan was born in Neptune, New Jersey on March 5, 1953. He graduated from Manasquan High School in Manasquan, New Jersey in June 1971. In September, 1971 he attended Rutgers University where he received his Bachelor of Arts Degree in Chemistry in January, 1976. In August, 1976 he came to Louisiana State University in Baton Rouge, where he is now a candidate for the degree of Doctor of Philosophy in the Department of Chemistry.

DOCTORAL EXAMINATION AND DISSERTATION REPORT

Candidate: John C. Hogan

Major Field: Chemistry

Title of Dissertation: Transition-structure Recognition in Polyether-catalyzed Ester Aminolysis Carried Out in Nonpolar Media

Approved:

Richard D. Gandour
Major Professor and Chairman

Dean of the Graduate School

EXAMINING COMMITTEE:

David L. Hala

Norman J. Blacco

Andrew W. Ewanowski

Mark L. McKee

Joanne K. Danilloff

Date of Examination:

November 8, 1990